

THE STUDY OF SPECTRAL ENERGY TRANSFER

IN $\text{La}_{1-x}\text{Pr}_x\text{P}_5\text{O}_{14}$

By

ROBERT BRUCE RUOKOLAINEN

Bachelor of Science
Eastern Michigan University
Ypsilanti, Michigan
1974

Master of Science
Eastern Michigan University
Ypsilanti, Michigan
1980

Submitted to the Faculty of the Graduate College
of the Oklahoma State University
in partial fulfillment of the requirements
for the Degree of
MASTER OF SCIENCE
December, 1982



"Everything Not Compulsory is Forbidden"

T. H. White, The Book of Merlin

From R. A. Wilson's "Schroedinger's Cat"

THE STUDY OF SPECTRAL ENERGY TRANSFER

IN $\text{La}_{1-x}\text{Pr}_x\text{P}_5\text{O}_{14}$

Thesis Approved:

Richard C. Powell

Thesis Adviser

Larry E. Halliburton

[Signature]

Norman N. Durha

Dean of the Graduate College

ACKNOWLEDGMENTS

I would like to thank my thesis adviser, Dr. R. C. Powell, for his guidance throughout this endeavor. Thanks are extended to the members of my committee, Dr. L. E. Halliburton and Dr. G. P. Summers, for their help and advice. My appreciation goes to other faculty members and graduate students for their helpful discussions.

TABLE OF CONTENTS

Chapter	Page
I. INTRODUCTION	1
II. A REVIEW OF ENERGY TRANSFER THEORY	3
Introduction	3
Single Step Energy Transfer	3
Phonon-Assisted Energy Transfer	6
Transfer to Random Sites	9
Multistep Energy Migration	9
III. EXPERIMENTAL METHOD	14
IV. EXPERIMENTAL RESULTS AND THEORETICAL ANALYSIS	21
Introduction	21
La _{0.5} Pr _{0.5} P ₅ O ₁₄ Analysis	22
PrP ₅ O ₁₄ Analysis	38
La _{0.9} Pr _{0.1} P ₅ O ₁₄ Analysis	45
V. SUMMARY AND CONCLUSIONS	54
REFERENCES	56

LIST OF TABLES

Table	Page
I. Excitation and Emission Lines of $\text{La}_{.5}\text{Pr}_{.5}\text{P}_5\text{O}_{14}$	18
II. Ratio of Intensities and Time After Pulse for $\text{La}_{.5}\text{Pr}_{.5}\text{P}_5\text{O}_{14}$ at 12K.	26
III. Ratio of Intensities and Time After Pulse for $\text{La}_{.5}\text{Pr}_{.5}\text{P}_5\text{O}_{14}$ at 50K.	36
IV. Ratio of Intensities and Time After Pulse for $\text{PrP}_5\text{O}_{14}$ at 12K	42
V. Ratio of Intensities and Time After Pulse for $\text{PrP}_5\text{O}_{14}$ at 48K	48
VI. Ratio of Intensities and Time After Pulse for $\text{La}_{.9}\text{Pr}_{.1}\text{P}_5\text{O}_{14}$	53

LIST OF FIGURES

Figure	Page
1. Excitation and Emission Apparatus.	16
2. Energy Level Diagram of Pr^{43} Ions in $\text{La}_{.5}\text{Pr}_{.5}\text{P}_5\text{O}_{14}$ at 12K.	17
3. TRS Apparatus.	20
4. Fluorescence Spectra of $\text{La}_{.5}\text{Pr}_{.5}\text{P}_5\text{O}_{14}$ at Two Different Excitation Wavelengths at $T = 25\text{K}$ and $t_{\text{ap}} = 550 \text{ ns}$	24
5. Spectral Dependence on Time After Pulse for $\text{La}_{.5}\text{Pr}_{.5}\text{P}_5\text{O}_{14}$ at 12K and $\lambda_x = 4816\text{\AA}$	25
6. Time Evolution of the Ratio of the Intensities for $\text{La}_{.5}\text{Pr}_{.5}\text{P}_5\text{O}_{14}$ at 12K	27
7. Interacting Two-Level System to Model Energy Transfer.	28
8. Proposed Energy Transfer Model for $\text{La}_{.5}\text{Pr}_{.5}\text{P}_5\text{O}_{14}$ at 12K.	31
9. Spectral Dependence on Time After Pulse for $\text{La}_{.5}\text{Pr}_{.5}\text{P}_5\text{O}_{14}$ at 50K and $\lambda_x = 4816\text{\AA}$	33
10. Time Evolution of the Ratio of the Intensities for $\text{La}_{.5}\text{Pr}_{.5}\text{P}_5\text{O}_{14}$ at 50K	35
11. Proposed Energy Transfer Model for $\text{La}_{.5}\text{Pr}_{.5}\text{P}_5\text{O}_{14}$ at 50K and $\text{PrP}_5\text{O}_{14}$ at 12K	37
12. Spectral Dependence on Time After Pulse for $\text{PrP}_5\text{O}_{14}$ at 12K and $\lambda_x = 4812\text{\AA}$	40
13. Fluorescence Spectra of $\text{PrP}_5\text{O}_{14}$ at Two Different Excitation Wavelengths and $t_{\text{ap}} = 214 \text{ ns}$	41
14. Time Evolution of the Ratio I_H/I_L for $\text{PrP}_5\text{O}_{14}$ at 12K	43
15. Time Evolution of the Ratio I_L/I_S for $\text{PrP}_5\text{O}_{14}$ at 12K	44
16. Spectral Dependence on Time After Pulse for $\text{PrP}_5\text{O}_{14}$ at 48K and $\lambda_x = 4812\text{\AA}$	46
17. Time Evolution of the Ratio I_L/I_H for $\text{PrP}_5\text{O}_{14}$ at 48K	47

Figure	Page
18. Fluorescence Spectra of $\text{La}_{0.9}\text{Pr}_{0.1}\text{P}_5\text{O}_{14}$ at Two Different Excitation Wavelengths at $t_{\text{ap}} = 278 \text{ ns}$	49
19. Spectral Dependence on Time After Pulse for $\text{La}_{0.9}\text{Pr}_{0.1}\text{P}_5\text{O}_{14}$ at 12K and $\lambda_x = 4806\text{\AA}$	50
20. Time Evolution of the Ratio I_H/I_L for $\text{La}_{0.9}\text{Pr}_{0.1}\text{P}_5\text{O}_{14}$ at 12K .	52

CHAPTER I

INTRODUCTION

Since the advent of the laser a new area of interest has developed in the field of optical spectroscopy, namely high resolution laser spectroscopy. This technique has enabled scientists to probe the structure of matter in much finer detail than previous methods.

This thesis is concerned with the specific procedure known as time resolved site selection spectroscopy. This method has been an invaluable tool in the study of energy transfer in solids. The site selection technique is conceptually very simple; a high resolution tunable dye pulse laser is used to selectively excite impurity atoms or ions in specific crystallographic field sites. By using the appropriate electronics, one can take spectral scans of impurity ion transitions at different times after the laser excitation pulse and observe the time-evolution of the entire fluorescence spectrum. This enables the investigator to determine the time dependence of the energy transfer and the number of excited atoms or ions involved in the transfer. This time dependence is accessible through the observation of fluorescent lifetimes and relative intensities of the fluorescing ions involved in the transfer. Moreover, one can determine the type of transfer mechanism and the strength of the interaction [1,2].

The characterization of energy transfer is critically important in developing efficient laser materials [1]. According to Yariv, the over-

all laser efficiency depends upon the fraction of the total pump power that is effective in transferring atoms into those states that lie above the metastable upper laser level and on the pump quantum efficiency defined as the fraction of the atoms that are in the higher excited state (i.e., higher than the metastable upper laser level) that make the transition to the metastable upper laser level [3]. It is here that the non-radiative energy transfer can enhance or quench the pumping efficiency of the active ions of the laser material.

Lanthanum praseodymium pentaphosphate is a potential laser material. In general, the trivalent lanthanide ions are used extensively for optically-pumped solid state lasers because they possess suitable absorption bands and numerous fluorescence lines of high quantum efficiency, in the visible and near-infrared [4]. An example of an extensively investigated trivalent lanthanide material is $\text{La}_{1-x}\text{Nd}_x\text{P}_5\text{O}_{14}$, $0 \leq x \leq 1$, but much less is known about the other pentaphosphates. As a result of this hiatus, work on $\text{La}_{1-x}\text{Pr}_x\text{P}_5\text{O}_{14}$ has been increasing during the past few years. Notable is the investigations of Dornauf and Heber on the fluorescence of Pr^{+3} -ions in $\text{La}_{1-x}\text{Pr}_x\text{P}_5\text{O}_{14}$ [5], and the concentration-dependent fluorescence-quenching in $\text{La}_{1-x}\text{Pr}_x\text{P}_5\text{O}_{14}$ [6].

CHAPTER II

A REVIEW OF ENERGY TRANSFER THEORY

Introduction

When material is exposed to a source of radiation, one kind of atom or ion in the material can absorb some of this radiation and be put into an excited state. Sometimes this excited state can give up its excitation not by radiative decay but by transferring its excitation to another atom or ion by a process referred to as radiationless energy transfer.

This process may be thought of as a quantum mechanical resonance between the interacting ions where a virtual photon is exchanged. The transfer mechanism can either be an electromagnetic multipole-multipole interaction or an exchange interaction [1].

The atoms or ions that initially absorb the energy are referred to as sensitizers and those atoms or ions that are "transferred to" are called activators. The activators may then give up their excitation in the form of light or heat. The sensitizers and activators may be the same species of ions, where they are delineated by slightly different crystallographic sites or they may be entirely different ions also influenced by the local crystal environment.

Single Step Energy Transfer

When the sensitizer is in an excited state and gives it excitation

directly to the activator, it is called single step energy transfer. If there is no energy mismatch between the sensitizer and activator transitions then it is referred to as single-step resonant energy transfer. This single step process dominates whenever the sensitizer concentration is very low or when the sensitizer-activator interaction is much stronger than the sensitizer-sensitizer interaction [1].

The electromagnetic interaction between the sensitizer and activator is responsible for the energy transfer. Transfer via electric dipole-dipole interaction was first described by Förster [8], and later Dexter [9] expanded the treatment to include higher order electromagnetic and exchange interactions [7].

The energy transfer rate for dipole-dipole interaction is given by [8]

$$\omega_{sa}^{DD} = (\tau_s^0)^{-1} (R_0/R_{sa})^6 \quad (1)$$

where τ_s^0 is the intrinsic lifetime of the sensitizer, R_{sa} is the sensitizer-activator separation, and R_0 is the critical interaction distance which is the sensitizer-activator separation at which the energy transfer rate is equal to the intrinsic decay rate.

Similar expressions can be derived for the energy transfer by other types of interaction i.e., electric dipole-quadrupole and quadrupole-quadrupole [7]. These interactions are related to the dipole-dipole transfer rate by [9]

$$\omega_{sa}^{DQ} = (\lambda/R_{sa})^2 (f_Q/f_D) \omega_{sa}^{DD}$$

and

$$\omega_{sa}^{QQ} = (\lambda/R_{sa})^4 (f_Q/f_D)^2 \omega_{sa}^{DD}$$

where λ is the wavelength of the transition, f_D is the oscillator strength of the dipole interaction, and f_Q is the oscillator strength of the quadrupole interaction. Transfer by these higher order multipole processes can be important if electric dipole transitions are forbidden.

If one assumes hydrogen-like electronic wave functions, the expression for energy transfer for the exchange interaction is given by [9,10]

$$\omega_{sa}^{EX} = (\tau_s^o)^{-1} \exp\{\delta[1 - (R_{sa}/R_o)]\}$$

where $\delta = 2R_o/L$ and L is the effective Bohr radius.

A general expression for the sensitizer population is given by [7]

$$n_s(t) = n_s(0) \exp\{-t/\tau_s^o - \Gamma(1 - 3/m)(N_a/C_o)(t/\tau_s^o)^{3/m}\}$$

where m is equal to 6, 8 or 10 for electric dipole-dipole, electric dipole-quadrupole and electric quadrupole-quadrupole interactions, respectively. For the exchange interaction the average energy transfer rate for the ensemble of sensitizers and activators is [10]

$$n_s(t) = n_s(0) \exp[-t/\tau_s^o - \delta^{-3}(N_a/C_o) g(e^{\delta} t/\tau_s^o)]$$

where

$$g(z) = -z \int_0^1 \exp(-zy) (\ln y)^3 dy .$$

Phonon-Assisted Energy Transfer

The rate of resonant energy transfer depends critically upon the energy mismatch between the sensitizer and activator transition. If there is a significant energy mismatch ΔE_{sa} between the sensitizer and activator transitions, the energy transfer rate can be negligibly small [7]. In this case energy transfer can occur through phonon-assisted processes [11,12].

The expression for one phonon assisted energy transfer is then [11]

$$\omega_{sa} = \frac{2\pi J^2 (f-g)^2}{\hbar(\Delta E_{sa})^2} \sum_{s,q} |\langle n_{s,q} \pm 1 | \epsilon | n_{s,q} \rangle|^2 h^I(\bar{q}, \bar{R}_{sa}) \delta(\hbar\omega_{s,q} \pm \Delta E_{sa}) \quad (2)$$

where the coherence factor $h^I(\bar{q}, \bar{R}_{sa})$ is given by

$$h^I(\bar{q}, \bar{R}_{sa}) = |\exp(i\bar{q} \cdot \bar{R}_{sa}) - 1|^2$$

which measures the degree to which a phonon mode causes the sensitizer to activator to move in or out of phase with each other. $(f-g)$ is the difference in coupling strengths, $n_{s,q}$ is the occupation number for the phonons and ϵ the strain operator which is written as a tensor (see reference 11, page 44, Eq. 2.5). J is the ion-ion matrix element taken to be independent of the phonon state and is expressed as

$$J = \langle s, a^* | H_{s-s} | s^*, a \rangle$$

where $*$ denotes excited state, s = sensitizer, a = activator and H_{s-s} is the site-site Hamiltonian which is multipolar or exchange interaction.

We now show the form of Eq. (2) for two cases, large energy mismatch and small energy mismatch.

i) Large energy mismatch:

The energy mismatch is large so $\bar{q} \cdot \bar{R}_{sa} > 1$ and the wavelength of the phonons is shorter than the separation between sensitizer and activator. A Debye distribution of phonon modes can be used to evaluate the sum in Eq. (2) and the coherence factor averages to approximately 2, then Eq. (2) becomes [11]

$$\omega_{sa} = \frac{J^2 (f-g)^2 |\Delta E_{sa}|}{\pi \hbar^4 \rho} \sum_s \frac{\alpha_s}{v_s^5} \begin{bmatrix} n_{sq} + 1 \\ n_{sq} \end{bmatrix} \quad (3)$$

for $\left[\begin{smallmatrix} \text{emission} \\ \text{absorption} \end{smallmatrix} \right]$ of a phonon of energy ΔE_{sa} , where ρ is the density, v_s is the phonon velocity, α_s involves the angular average of the strain parameter, and

$$n_{sq} = [\exp(\Delta E_{sa}/k_B T) - 1]^{-1}$$

If $\Delta E_{sa} < k_B T$ then Eq. (3) reduces to [11]

$$\omega_{sa} = \frac{J^2 (f-g)^2}{\pi \hbar^4 \rho} \sum_s \frac{\alpha_s}{v_s^5} k_B T$$

It is seen that the one-phonon-assisted transfer rate is independent of the energy mismatch and linearly dependent on temperature.

ii) Small energy mismatch:

When the energy mismatch is small, the quantity qR_{sa} becomes small and the coherence factor becomes approximately $(qR_{sa})^2/3$ and Eq. (2), following the same procedure as above becomes

$$\omega_{sa} = \frac{J^2 (f-g)^2 |\Delta E_{sa}|^3 R_{sa}^2}{6 \pi \rho \hbar^6} \sum_j \frac{\alpha_s}{v_s^7} \begin{bmatrix} n_{sq} + 1 \\ n_{sq} \end{bmatrix} \quad (4)$$

Again if $\Delta E_{sa} < k_B T$, then Eq. (4) reduces to

$$\omega_{sa} = \frac{J^2 (f-g)^2 |\Delta E_{sa}|^2 R_{sa}^2}{6 \pi \hbar^6 \rho} \sum_s \frac{\alpha_s}{v_s^7} k_B T \quad (5)$$

In general, Eq. (5) is smaller than the corresponding expression for large energy mismatch by the factor $(\Delta E_{sa} R_{sa} / v_s \hbar)^2$. Under the condition of energy transport between similar ions at small energy mismatch, Eq. (5) is in general too small to be observable, and higher order mechanics predominate [11].

These higher order processes are two phonon or multiphonon processes. The smallness of the coherence factor for small energy transfer and/or the small density of states when $|E_{sa}| \ll k_B T$, leads to consideration of higher order processes. These processes can dominate for two reasons [11].

- a) Limitation of the strength of the one-phonon-assisted process because of small phonon density of states ΔE_{sa} , and/or
- b) Lack of interference in the two-phonon-assisted coherence factor. The phonons involved in higher order processes have short wavelengths $\lambda \approx 2\pi \hbar v_s / k_B T$, and, as a consequence, cancellation in the interference factor is avoided.

(Higher order processes are described in detail in reference [7], page 53 and reference [11], Section 2.3.3).

Transfer to Random Sites [2]

If a crystal has a random distribution of both sensitizers and activator sites the rate of decay of an excited sensitizer is its radiative decay rate, τ , plus an energy transfer rate characteristic of its activator environment, i.e., all sensitizers with the same distribution of unexcited activators around them decay at the same rate.

The total rate of transfer from the excited sensitizer population n^* is

$$n^*(t) = kN_s \exp[-(1/\tau + \omega_r)t]$$

where k is the fraction of sensitizers originally excited, N_s the number of sensitizers and for an assumed dipole-dipole interaction

$$\omega_r = \omega_r(t) = 4\pi^{3/2} R_0^3 C_a / 3(\tau t)^{1/2}$$

where $C_a = N_a/V$ the activator concentration.

Multistep Energy Migration

In multistep energy migration the energy travels many times between sensitizers before transfer to an activator occurs. This may occur if there are more sensitizers than activators in the crystal. Each energy transfer step can be treated by one of the previously discussed ion-ion interaction mechanisms. This may be either the same as or different from the mechanism of sensitizer-activator interaction. In characterizing this type of energy transfer it is important to describe both the dynamics of the process of migration among the sensitizers and the trapping of the energy at the activator site. There are two mathematical

approaches to multistep energy migration theory, one is based on a random walk model and the other on diffusion. In the limit of many steps in the random walk on a uniform three dimensional lattice, the two approaches are equivalent [7].

In the diffusion formalism, the rate of change of the exciton population is [7]

$$\partial N(r,t)/\partial t = W(t) - \beta N(r,t) + DV^2 N(r,t) \quad (6)$$

where $N(r,t)$ is the exciton concentration, β is the sensitizer decay rate, D the diffusion coefficient, and $W(t)$ is the rate of excitation of sensitizers. With the appropriate boundary conditions viz.,

$$N(r,t = 0) = N_0$$

$$N(r = R_T, t) = 0$$

where R_T is the trapping radius and using the substitution

$$N(r,t) = [U(r,t)/r]\exp(-t\beta)$$

and then using Laplace transforms on Eq. (6) the solution is [7]

$$N(r,t) = N_0 \{1 - (R_T/r) \operatorname{erfc}[(r - R_T)/2D^{1/2}t^{1/2}]\} \exp(-t\beta)$$

The energy transfer rate can be derived by considering a flux of excitons crossing a spherical surface of a single trap [7]

$$F(t) = 4\pi DR_T^2 \left[\frac{\partial N}{\partial t} \right]_{r=R_T}$$

For C_T non-interacting traps

$$F_N(t) = 4\pi DC_T \exp(-t\beta) [R_T + R_T^2/(\pi Dt)^{\frac{1}{2}}]$$

Thus the transfer rate is

$$\omega_D = 4\pi DR_T C_T [1 + R_T/(\pi Dt)^{\frac{1}{2}}] \quad (7)$$

The point trapping approximation used here does not sufficiently describe the true physical situation, so Soos and Powell [13] extended the diffusion theory to include trapping regions of various sites and geometries. This model is suitable for cases where the energy transfer is dominated by diffusion of excitons into the trapping regions with no special interaction between excitons and traps. These trapping regions can occur when an activator is much larger than the ion or molecule it replaces, and thus distorting the lattice around the activator. The derivation of the energy transfer rate is similar to that of Eq. (7) and for a simple cubic lattice the rate becomes [7]

$$\omega_{sp} = \omega(\infty) [1 + (2C\{A\}v_m)/(4\pi D)^{3/2} t_h t^{\frac{1}{2}}]$$

where $\omega(\infty) = C_T v_m C\{A\} t_h^{-1}$

with t_h the hopping time, v_m as the volume per molecule of the host lattice and $C\{A\}$ the capacity of the random walk defined as the number of previously unsampled sites sampled by the exciton on each step of the random walk in the limit of many steps and A the number of lattice sites distorted by the activator.

Another approach is to include a host-activator interaction in the diffusion equation

$$\partial n_s(\bar{r}, t) / \partial t = -\beta n_s(\bar{r}, t) + D \nabla^2 n_s(\bar{r}, t) - \sum \omega_{sa}(\bar{r} - \bar{R}_i) n_s(\bar{r}, t) \quad (8)$$

where R_i is the position vector for a given activator and $\omega_{sa}(r - R_i)$ is the interaction strength for a given host ion-activator pair.

Eq. (8) was solved by Chow and Powell [14] for the case of fast diffusion with weak host-activator interaction with the assumption of a dipole-dipole mechanism. The transfer rate is given as [7]

$$\omega_{CP} = \omega_D + \omega_1$$

where ω_D is given by Eq. (7) and

$$\begin{aligned} \omega_1(t) = & 4\pi N_a \beta_s R_o^6 / 3R_T + 2\pi N_a R_T^2 \int_{R_T}^{\infty} dr (\beta_s R_o^6 / r^6) [\text{erfc}(r - R_T) / (4Dt)^{1/2}]^2 \\ & - 8\pi N_a \int_{R_T}^{\infty} dr (\beta_s R_o^6 / r^6) [\text{erfc}(r - R_T) / (4Dt)^{1/2}] \end{aligned}$$

Yokota and Tanimoto [15] solved Eq. (8) for the case of weak diffusion and strong host-activator interaction again for a dipole-dipole mechanism. Their result is

$$\begin{aligned} n_s(t) = & \exp\{-\beta_s t - N_a (4/3) \pi^{3/2} R_o^3 (\beta_s t)^{1/2} [(1 + 10.90 xt^{2/3} \\ & + 15.7 x^3 t^{4/3}) / (1 + 8.76 xt^{2/3})]\} \end{aligned}$$

where $x = D\beta_s^{-1/3} R_o^{-2}$

A last approach to treating trapping was developed by Burshtein [16] and is based upon treating the transfer rate as random variable in a stochastic hopping process. The sensitizer population is

$$n_s(t) = \bar{n}_s(t) \exp(-t/t_0) + t_0^{-1} \int_0^t n_s(t-t') \bar{n}_s(t') \exp(-t'/t_0) dt' \quad (9)$$

where t_0 is the average value of the hopping time and $n_s(t)$ is interaction dependent. Eq. (9) can only be solved for limiting cases which will not be discussed here.

CHAPTER III

EXPERIMENTAL METHOD¹

The first part of this experiment was to determine the excitation and emission spectra of the samples, at room temperature and low temperature (i.e., ~12K), thus enabling one to choose the laser excitation wavelength and the region of the emission spectrum to be investigated.

The excitation spectra were obtained using a tungsten halogen lamp as a source. The light was focused onto the entrance slit of a Spex Model 1670 minimate monochromator, with slit width typically 1.25 mm to 2.50 mm. A short focal length lens focused the monochromator output onto the sample. A Spex one meter Czerny-Turner spectrometer was used to analyze the fluorescent output of the sample. This spectrometer, the Model 1704, has a 4\AA per mm dispersion and a resolution better than 0.1\AA , and was used with slit widths of about 0.25 mm. To detect the signal, an RCA C31034 phototube cooled by a Products for Research thermoelectrically refrigerated chamber, Model TE-104, was mounted on the exit slit of the spectrometer. The input signal to the spectrometer was chopped by a PAR Model 125 mechanical chopper. The output of the phototube was amplified by a PAR Model 128 Lock-in Amplifier and, of course, the light chopper was used as a reference signal. The spectra were recorded on a Heath strip chart recorder. For low temperature work the

¹Part of the experimental method is based upon Reference 2.

sample was mounted on the cold finger of an Air Products and Chemicals Model CS-202 Displex Cryogenic Refrigerator. This closed cycle helium refrigerator attains temperatures of 12K. A block diagram of the experimental set-up is shown in Figure 1.

An energy level diagram for $\text{La}_{.5}\text{Pr}_{.5}\text{P}_{.5}\text{O}_{14}$ at 12K is constructed in Figure 2. It is based upon the excitation and emission lines listed in Table I, which were determined from the above technique and the aid of Dornauf and Heber's paper [5].

The second part of the experiment involved the collection of fluorescence and lifetime measurements for a range of low temperatures, e.g. 12K to approximately 60K. From this information one can begin to model the energy transfer mechanism.

The fluorescence spectra and lifetime measurements were made using a Molelectron DL II dye laser pumped by a Molelectron UV 14 pulsed nitrogen laser as the excitation source. The dye employed was an Exciton, Inc., product called LD 466. The solvent for the dye was ethanol. The spectral range of the dye is 446 nm to 492 nm, with a maximum at 464 nm. The laser output was focused onto the sample (mounted in the cryostat) using a 2.5 cm focal length lens. The cryogenic refrigerator used here is the same unit used in the excitation/emission work. The fluorescence signal was focused onto the Spex one meter spectrometer with slit widths ranging from 10.0 microns to 25.0 microns.

The phototube signal was processed by a Model 162 Boxcar Averager with a Model 165 gated integrator (processor module) made by the Princeton Applied Research Corp. For fluorescence spectral measurements, the 165 processor module when triggered by the pulse laser samples the phototube signal during a narrow aperture which is fixed at a certain

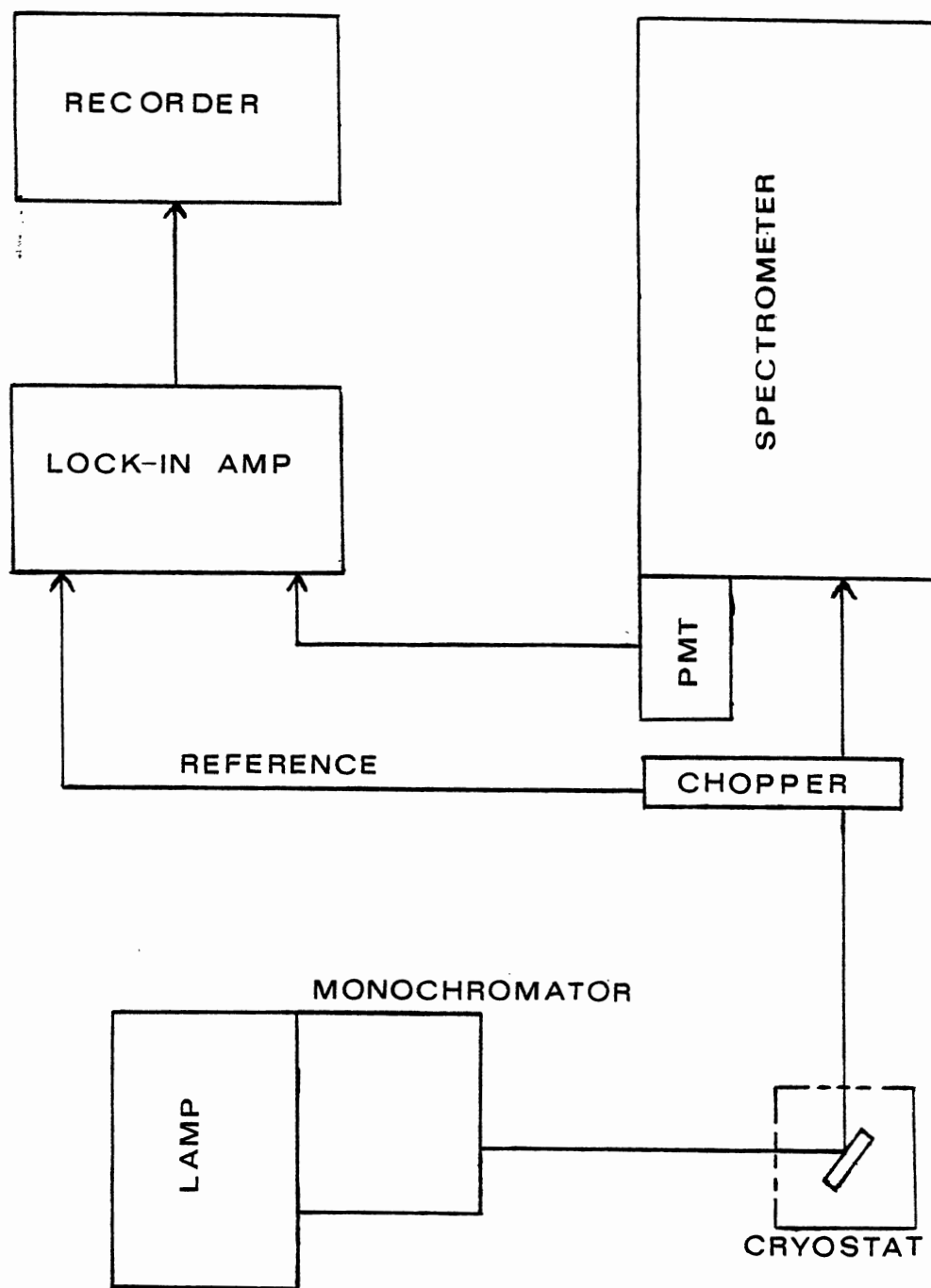


Figure 1. Excitation and Emission Apparatus

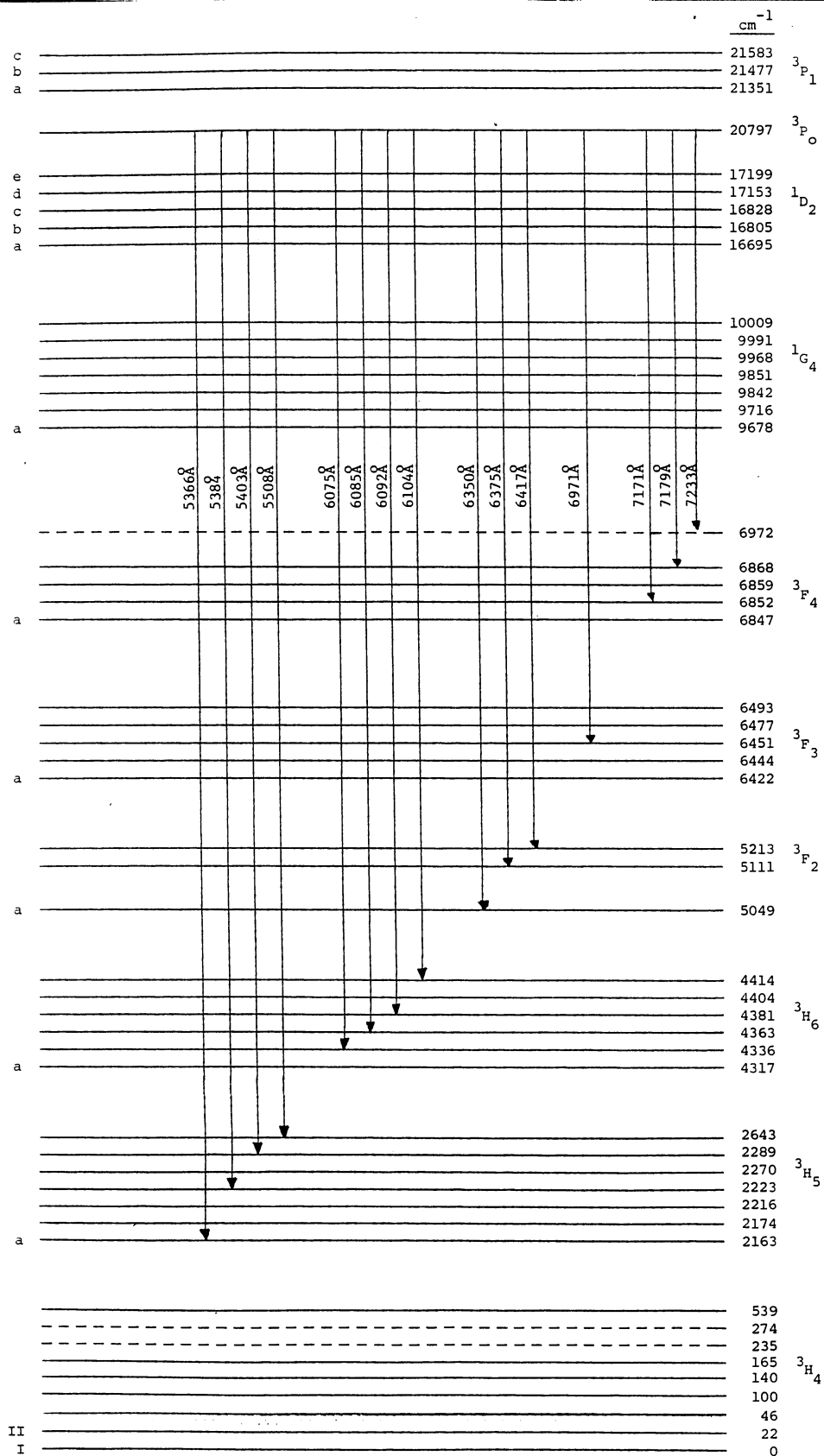


Figure 2. Energy Level Diagram of Pr^{+3} Ions in $\text{La}_{.5}\text{Pr}_{.5}\text{P}_5\text{O}_{14}$ at 12K

TABLE I
 EXCITATION AND EMISSION LINES OF $\text{La}_{.5}\text{Pr}_{.5}\text{P}_5\text{O}_{14}$

Transition	λ (Å)	$\tilde{\nu}$ (cm^{-1})
Excitation:		
I ${}^3\text{H}_4 \rightarrow {}^3\text{P}_1$	4416	22645
	4458	22432
	4647	21519
II ${}^3\text{H}_4 \rightarrow {}^3\text{P}_0$	4816	20764
I ${}^3\text{H}_4 \rightarrow {}^1\text{D}_2$	5574	17940
Emission:		
${}^3\text{P}_0 \rightarrow {}^3\text{H}_5$	5366.7	18634
	5384	18574
	5403	18508
	5508.3	18154
${}^3\text{P}_0 \rightarrow {}^3\text{H}_6$	6075	16461
	6085	16434
	6091.7	16416
	6104	16383
${}^3\text{P}_0 \rightarrow {}^3\text{F}_2$	6350	15748
	6375	15686
	6416.7	15584
${}^3\text{P}_0 \rightarrow {}^3\text{F}_3$	6970.8	14346
${}^3\text{P}_0 \rightarrow {}^3\text{F}_4$	7170.8	13945
	7179.1	13929
	7233.3	13825

time after the laser pulse. For different times after pulse settings on the boxcar, scan is made with the spectrometer. The output of the boxcar was plotted on the Heath strip chart recorder. For lifetime measurements, the processor module (triggered by the laser) scans the narrow aperture across a wide time range for a fixed fluorescence wavelength of the spectrometer. The output in this case was plotted on a Houston Instruments x-y recorder.

In both types of measurements the signal that passes the narrow aperture is sampled many times so that the output of the boxcar is the average of a number of pulses of the input signal, thus improving the signal to noise ratio.

Settings for the 165 processor module were an input resistance of 50 ohms, time constant was either 0.5 microseconds or 1.0 microseconds. The aperture duration, set on the boxcar mainframe or the module, depending on the width desired, was 50 nanoseconds. The mainframe time constant was 0.1 milliseconds.

A block diagram of the experimental set up for time resolved spectroscopy (TRS) is shown in Figure 3. The excitation wavelength of the laser was approximately $4816\overset{\circ}{\text{Å}}$ and a bandwidth of $0.3\overset{\circ}{\text{Å}}$. This wavelength pumps the II $^3\text{H}_4 \rightarrow ^3\text{P}_0$ transition of the Pr^{3+} ions in $\text{La}_{.5}\text{Pr}_{.5}\text{P}_5\text{O}_{14}$. The remaining samples were excited with wavelengths close to $480\overset{\circ}{\text{Å}}$. The fluorescence spectra had peaks in the $6072\overset{\circ}{\text{Å}}$ region and the scan usually covered a wavelength range from $6065\overset{\circ}{\text{Å}}$ to $6085\overset{\circ}{\text{Å}}$.

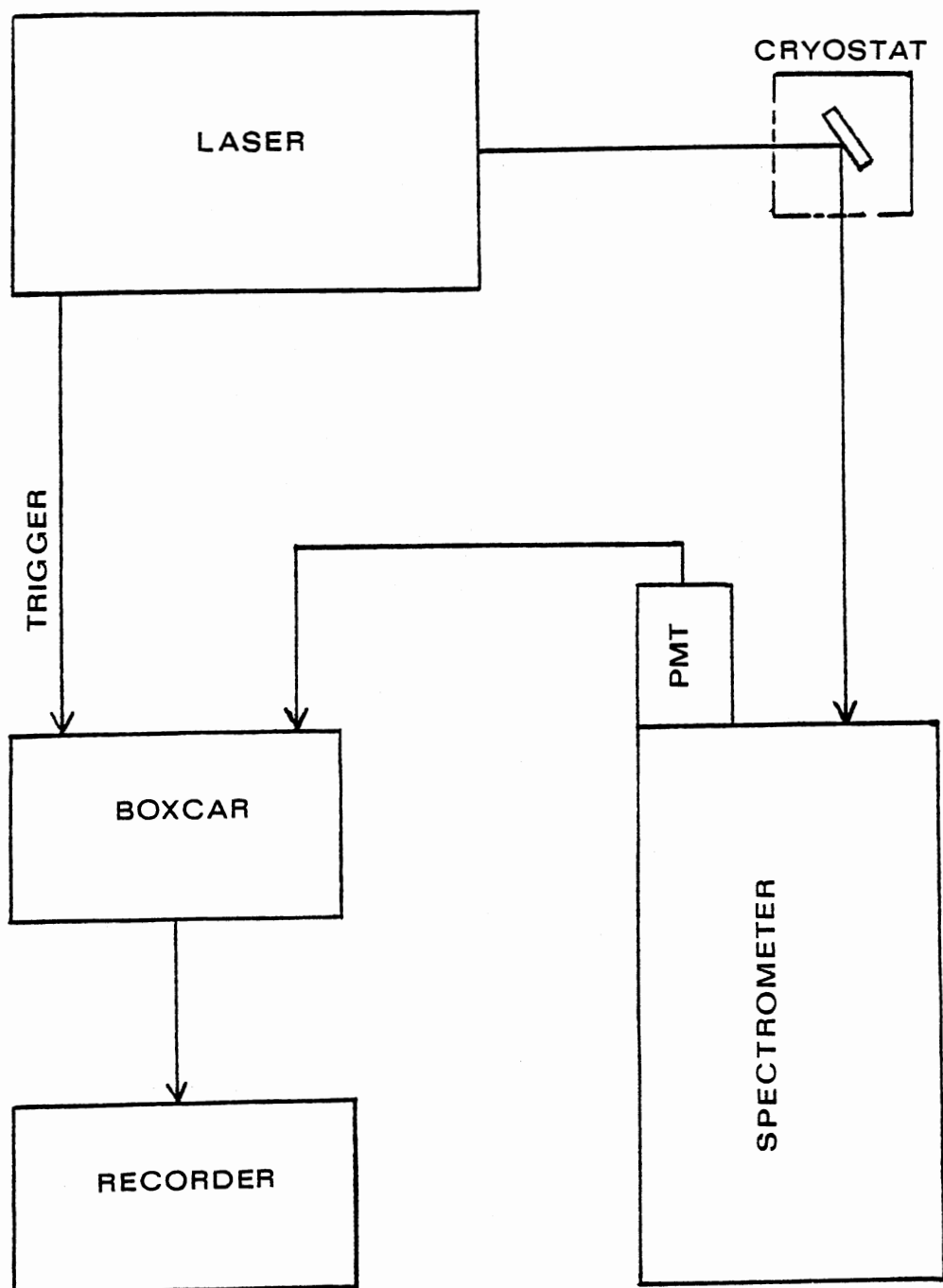


Figure 3. TRS Apparatus

CHAPTER IV

EXPERIMENTAL RESULTS AND THEORETICAL ANALYSIS

Introduction

In this chapter each sample is given a section in which it is discussed in terms of its method of analysis, lifetimes, time dependence of the spectra at high and low temperatures, time evolution of the ratio of the intensities, energy transfer model and solution of the rate equations.

The determination of the energy transfer parameters is based upon the energy transfer model chosen and the rate equations describing the situation. The analysis is either carried out on an LSI-11 computer using fitting routines or using the computer as a calculator to "hand fit" the data.

The models used in energy transfer are phenomenological in nature and it can be the case that more than one of the theoretical models can generally give a good fit to a specific set of data. Thus, identification of the correct model cannot be based solely on achieving a good fit. The energy transfer parameters obtained from the fitting procedure must satisfy the validity criteria for the model. These criteria and the transfer parameters reflect the microscopic kinetics of the energy transfer which are important elements in determining the appropriate phenomenological model to use in interpreting the data [17].

The samples investigated were mixed crystals of $\text{La}_{.5}\text{Pr}_{.5}\text{P}_5\text{O}_{14}$ and $\text{La}_{.9}\text{Pr}_{.1}\text{P}_5\text{O}_{14}$ where the Pr^{3+} ions substitute for the La^{3+} ions or equally the La^{3+} ions substitute for the Pr^{3+} sites, and a stoichiometric sample $\text{PrP}_5\text{O}_{14}$. The pentaphosphates crystallize in three different structures; for our samples it is monoclinic with the space group P_2^1/a . Since the angle β is close to 90 degrees it is also referred to as pseudo-orthorhombic structure [5].

$\text{La}_{.5}\text{Pr}_{.5}\text{P}_5\text{O}_{14}$ Analysis

This sample exhibits a spectrum which consists of two peaks, the high energy peak at $6070\overset{\circ}{\text{A}}$, the low energy peak at $6072\overset{\circ}{\text{A}}$ and the area between the peaks which intimately connects the two peaks which is due to the fluorescing ions in the continuum. The contribution of the continuum to the spectrum at low temperature is localized between the peaks; whereas in the high temperature case, 50K, the continuum becomes a prominent feature of the spectrum, i.e., the spectrum becomes a broadband with peaks protruding from the broadband. This is probably due to more efficient energy transfer and thermal broadening.

Because the area between the peaks showed change for different times after a pulse it was decided to symmetrize the two peaks, determine their areas, then sum the overlapping wings of the two peaks, and then determine the remaining area, thus there are three integrated intensities to be dealt with; I_H the intensity of the high energy peak, I_L the intensity of the low energy peak, and I_I the intensity of the intermediate fluorescing sites.

The laser excitation wavelength was approximately $4816\overset{\circ}{\text{A}}$ which pumps the $\text{II } ^3\text{H}_4 \rightarrow ^3\text{P}_0$ transition of the Pr^{3+} ions. The emission spectrum is

due to the ${}^3P_0 \rightarrow {}^3H_6$ transition of the Pr^{3+} ions. The lifetime of I_H and I_I at 12K are 74 ns and 71 ns, respectively, and that of I_L is 98 ns. At 50K the lifetime of the I_L peak is 68 ns.

Shown in Figure 4 is the fluorescence spectrum between 6063\AA and 6078\AA at 25K and 550 ns after the excitation pulse. As seen in the figure the position of the emission line changes significantly and to a lesser extent the shape changes as the laser excitation wavelength is changed by approximately one angstrom. This is due to selectively exciting the Pr^{3+} ions in nonequivalent crystal field sites having slightly different transition energies for both absorption and emission. Figure 5 shows the time evolution of the spectral region $6065\text{\AA} - 6080\text{\AA}$ at 12K for two times after excitation pulse. The excitation wavelength selectively excites the ions giving rise to the high energy transition, the low energy transition, and the intermediate sites and the spectral intensity evolves to the intermediate sites with time.

The energy transfer from sensitizers (Pr^{3+} ions in sites producing the high and low energy transitions) to the activators (Pr^{3+} ions in sites producing the intermediate energy transitions) can be characterized by monitoring the time dependence of their relative fluorescence intensities. The ratio of the integrated fluorescence intensities of the activator and sensitizer transitions, viz. $I_I/(I_H + I_L)$, is plotted in Figure 6 for a temperature of 12K. Table II gives a listing of the ratios of intensities for different times after pulse.

Attempts were made to fit the time dependent data in Figure 6 using two different aspects of the interacting two-level system model shown in Figure 7. The rate equations for the populations of excited states of the two sites can be written [18]

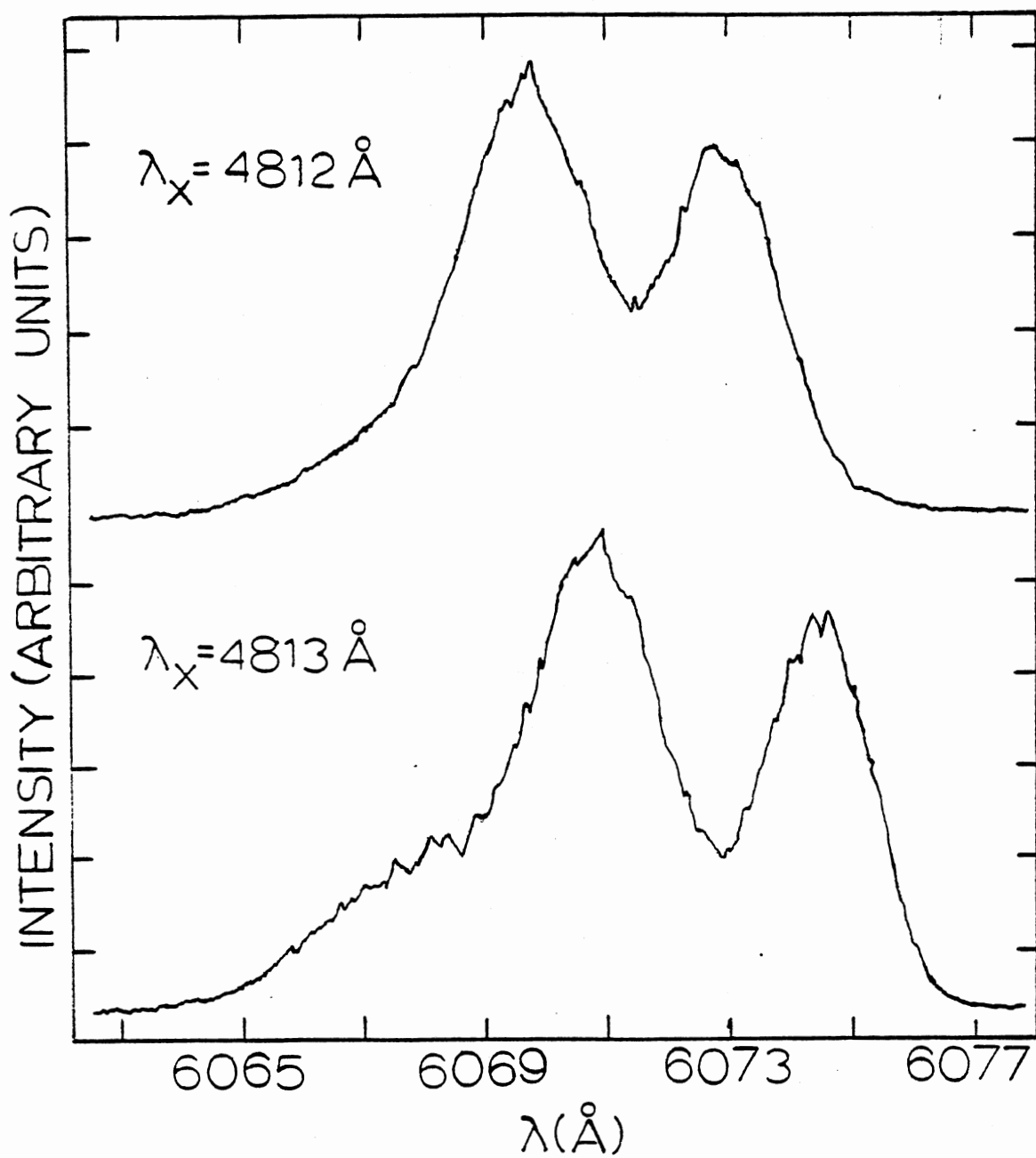


Figure 4. Fluorescence Spectra of $\text{La}_{0.5}\text{Pr}_{0.5}\text{P}_5\text{O}_{14}$ at Two Different Excitation Wavelengths at $T=25\text{K}$ and $t_{\text{ap}}=550\text{ns}$

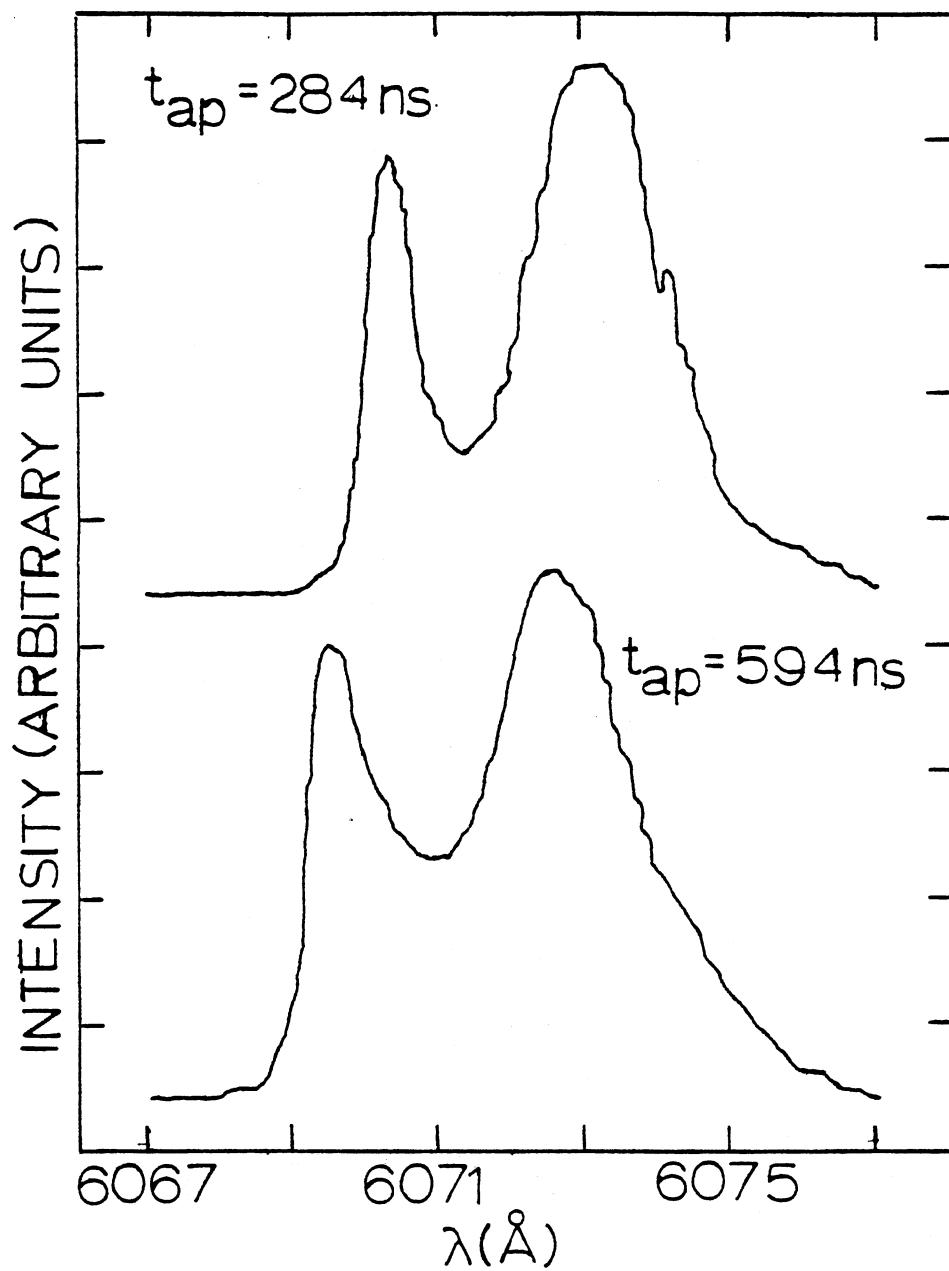


Figure 5. Spectral Dependence on Time After Pulse for $\text{La}_{0.5}\text{Pr}_{0.5}\text{P}_5\text{O}_{14}$ at 12K and $\lambda_x = 4816\text{\AA}$

TABLE II
RATIO OF INTENSITIES AND TIME AFTER PULSE
FOR $\text{La}_{.5}\text{Pr}_{.5}\text{P}_5\text{O}_{14}$ AT 12k

T_{ap} (ns)	$I_I / (I_H + I_L)$
284.0	0.0433
290.0	0.0450
296.0	0.0609
302.0	0.0783
308.0	0.1147
314.0	0.1113
320.0	0.1208
326.0	0.0892
346.0	0.1028
408.0	0.1529
420.0	0.1318
532.0	0.1526
594.0	0.1974

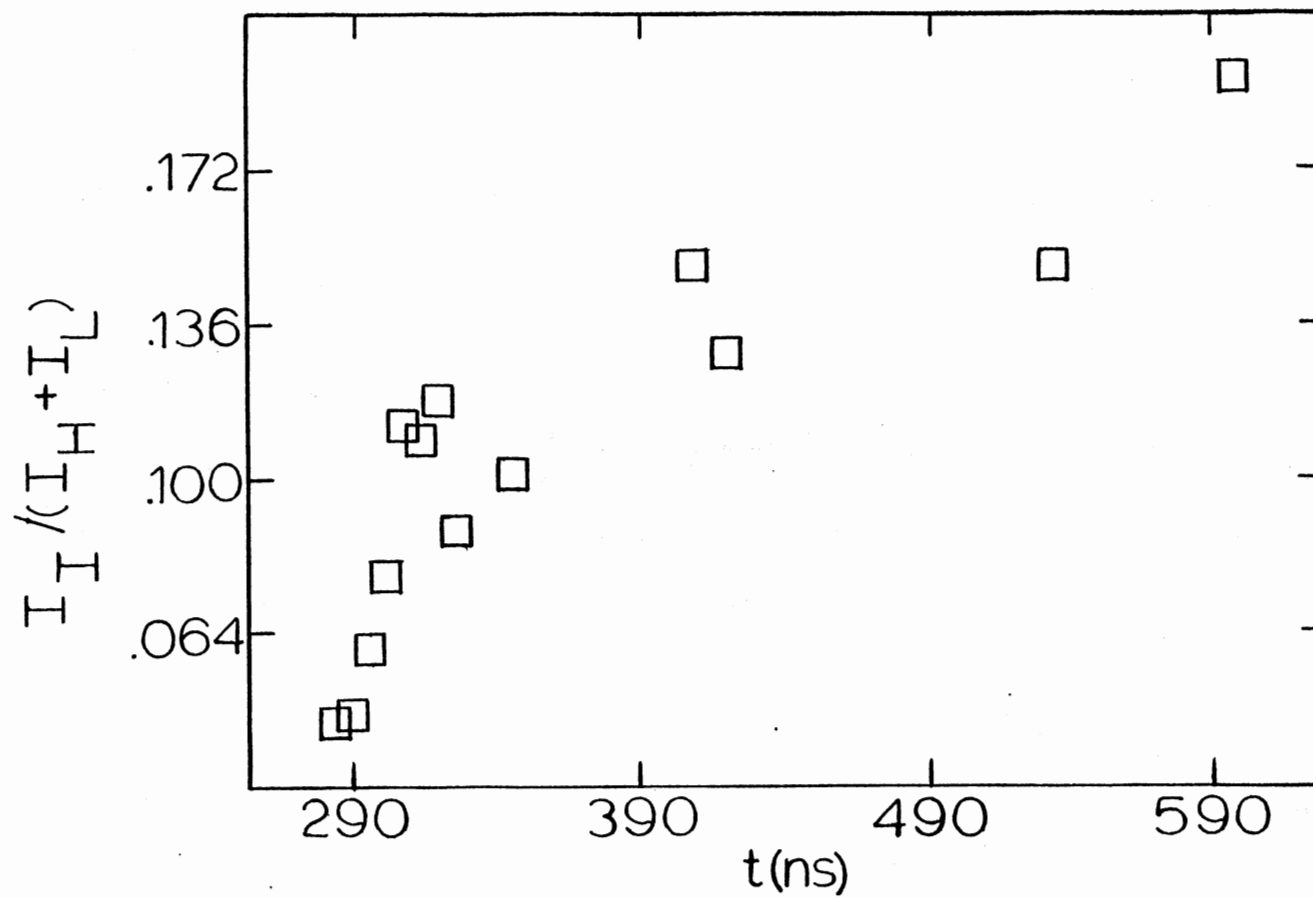


Figure 6. Time Evolution of the Ratio of the Intensities for $\text{La}_{.5}\text{Pr}_{.5}\text{P}_5\text{O}_{14}$ at 12K

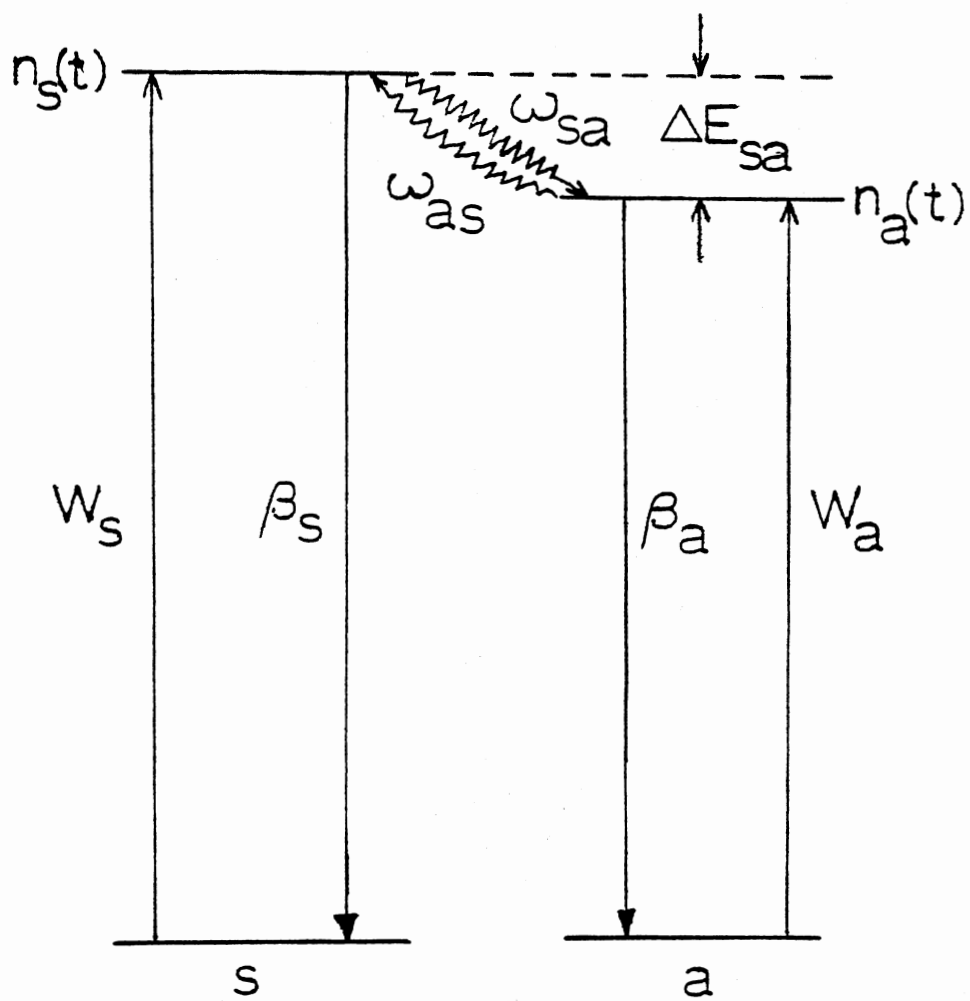


Figure 7. Interacting Two-Level System to Model Energy Transfer

$$\frac{dn_s}{dt} = W_s - \beta n_s - \omega_{sa} n_s + \omega_{as} n_a \quad (9a)$$

$$\frac{dn_a}{dt} = W_a - \beta n_a + \omega_{sa} n_s - \omega_{as} n_a \quad (9b)$$

where W_s and W_a are the pumping rates, β is the intrinsic fluorescence decay rate, ω_{sa} and ω_{as} are the energy transfer and back transfer rates between the sensitizer and activator sites, and ΔE (in the figure) is the energy mismatch between the excited levels of the ions in the two sites. In order to solve these equations a few assumptions are made; the pumping rates are treated as δ -functions, the transfer rates are time independent, and the lifetimes are equal. Under these conditions, solutions to Eqs. (9a) and (9b) lead to [19]

$$\frac{I_a(t)}{I_s(t)} = \frac{\frac{\omega_{sa}}{\omega_{as}} \left[\frac{n_a(0)}{n_s(0)} + 1 \right] - \left[\frac{\omega_{sa}}{\omega_{as}} - \frac{n_a(0)}{n_s(0)} \right] \exp[-(\omega_{sa} + \omega_{as})t]}{\left[\frac{n_a(0)}{n_s(0)} + 1 \right] + \left[\frac{\omega_{sa}}{\omega_{as}} - \frac{n_a(0)}{n_s(0)} \right] \exp[-(\omega_{sa} + \omega_{as})t]} \quad (10)$$

where $I_a(0)/I_s(0) = n_a(0)/n_s(0)$; $I(\infty)/I_s(\infty) = \omega_{sa}/\omega_{as}$. The attempts made at fitting the data of Table II to Eq. (10) using a fitting routine on the LSI-11 computer and hand calculations were unsuccessful.

Assuming δ -function excitation, negligible back transfer, equal values for the sensitizer and activator decay times, and a $t^{-1/2}$ dependence of the energy transfer rate, solutions to Eqs. (9a) and (9b) now become under these conditions [20]

$$I_a(t)/I_s(t) = \left[I_a(0)/I_s(0) + 1 \right] \exp[(2\gamma t^{-1/2})t] - 1 \quad (11)$$

where

$$\omega_{sa} = \gamma t^{-1/2} = \frac{4}{3}(\pi)^{3/2} R_{Oa}^3 N_s \beta_s^{1/2} t^{-1/2}$$

This type of time dependence for the energy transfer is typical for a single-step process between randomly distributed sensitizers and activators taking place by electric dipole-dipole interaction [10]. By taking the natural logarithm of the quantity of one plus the ratio of intensities did not vary linearly as $t^{1/2}$ (the proof is not presented here). Thus, this model did not fit the data listed in Table II.

I propose a third discrete site model consisting of an interacting three-level system as shown in Figure 8. Where H denotes high (for high energy peak), I for intermediate site(s), and L for low (in low energy peak). The rate equations for the populations of this system are

$$dn_H/dt = W_H - \beta_{HH} n_H - \omega_{HI} n_H \quad (12a)$$

$$dn_I/dt = W_I - \beta_{II} n_I + \omega_{HI} n_H + \omega_{LI} n_L \quad (12b)$$

$$dn_L/dt = W_L - \beta_{LL} n_L - \omega_{LI} n_L \quad (12c)$$

In this model as seen from the rate equations there is transfer from site H to site I but no back transfer between these sites, and only back transfer from site L to site I. In solving Eqs. (12), again the pumping rates are treated as δ -functions, the energy transfer rates are constant through this need not be necessary. By using the method of Laplace transforms the solution to Eqs. (12) under these conditions is

$$\frac{I_I}{I_H + I_L} = \frac{A \exp(\beta_L - \beta_I + \omega_{LI})t + B \exp(\beta_L - \beta_H + \omega_{LI} - \omega_{HI})t + C}{(\beta_H^r / \beta_I^r) \exp(\beta_I - \beta_H + \omega_{LI} - \omega_{HI})t + \beta_{LL}^r n_L(0) / \beta_{IH}^r n_H(0)} \quad (13)$$

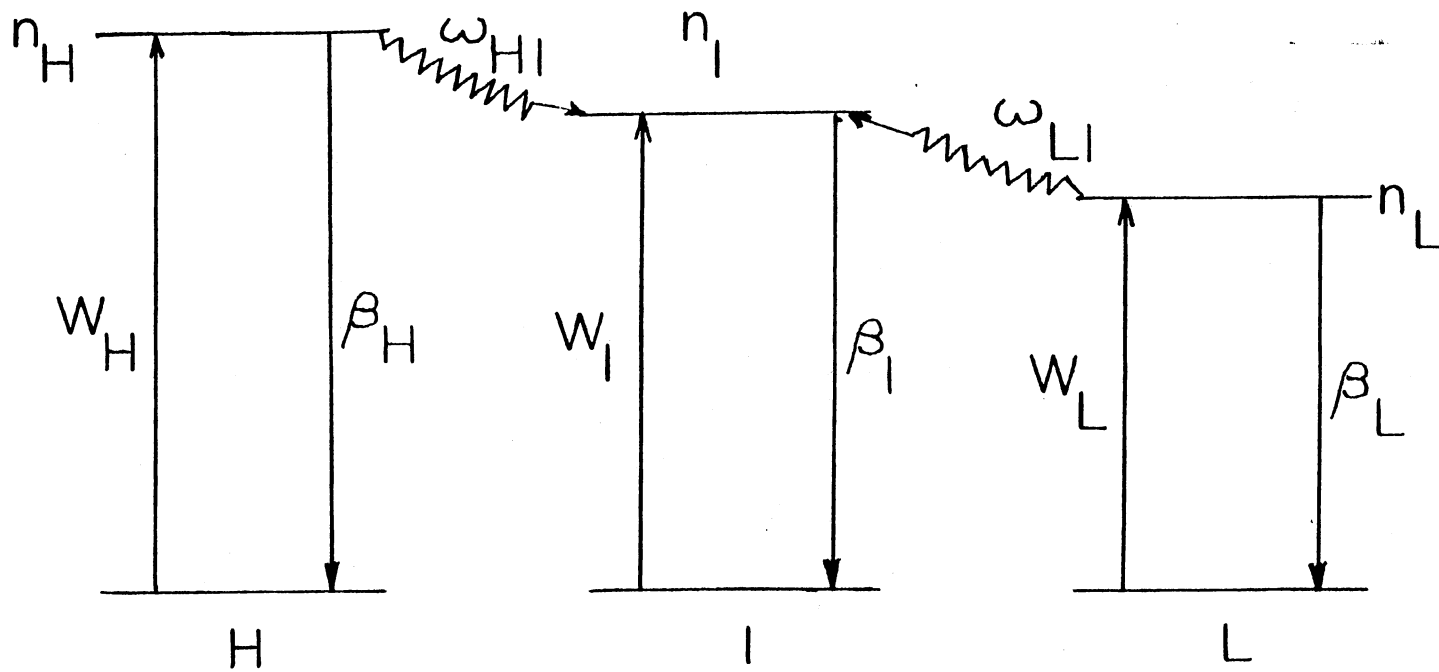


Figure 8. Proposed Energy Transfer Model for $\text{La}_{.5}\text{Pr}_{.5}\text{P}_2\text{O}_{14}$ at 12K

where

$$A = [n_L(0)/n_H(0)] - [n_L(0)\omega_{LI}/n_H(0)]/(\beta_I - \beta_L - \omega_{LI})$$

$$B = \omega_{HI}/(\beta_I - \beta_H - \omega_{HI})$$

$$C = [n_L(0)\omega_{LI}/n_I(0)]/(\beta_I - \beta_L - \omega_{LI})$$

and β^r 's are the radiative decay rates.

This model has features similar to the first model proposed, i.e., in the earlier model the high energy site and the low energy site were the sensitizers and the intermediate site was the activator. In the three discrete site model this is still true, but by modeling on three discrete sites we introduce added parameters, viz., the initial population ratios involving three sites, the radiative decay rates, and the fluorescence decay rates, which may help fit the data. The data presented in Table II and plotted in Figure 6 has yet to be fitted in Eq. (13).

The spectra of $\text{La}_{.5}\text{Pr}_{.5}\text{P}_5\text{O}_{14}$ at 50K are different than that of the 12K spectra. As noted before these spectra exhibit a broadband with peaks "growing out" of the band or in some cases the peaks are nearly absent depending on the time after excitation pulse. Figure 9 shows the spectral dependence on time after pulse for two different times after excitation pulse. This excitation wavelength excites ions in the continuum which correspond to band and nonband transitions and the spectral intensity evolves to band energy sites. At long times after pulse, the continuum of sites fluoresce to give the broadband spectrum with barely any peaks remaining, i.e., the traps are long lived. This type of

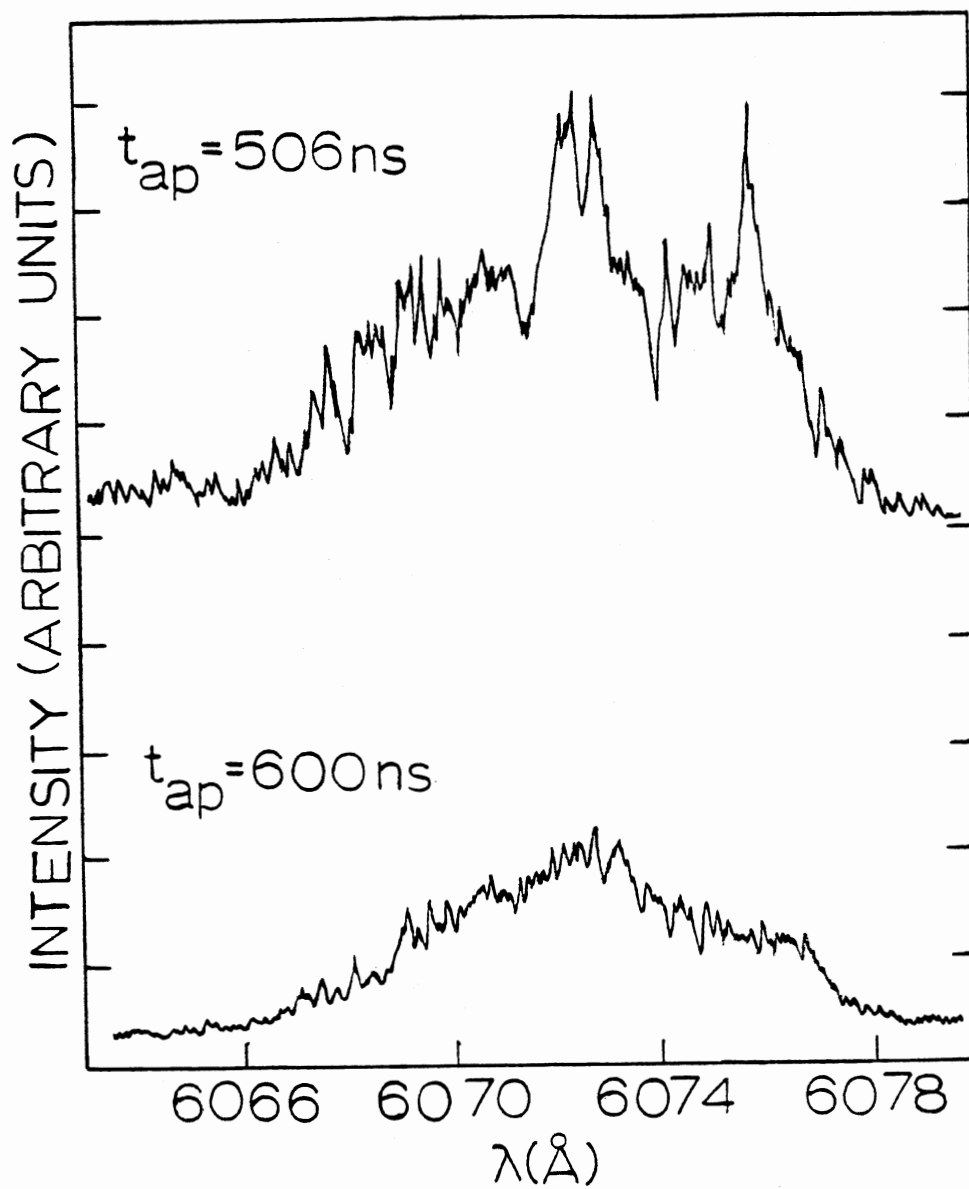


Figure 9. Spectral Dependence on Time After Pulse for $\text{La}_{.5}\text{Pr}_{.5}\text{P}_2\text{O}_{14}$ at 50K and $\lambda_x = 4816\text{\AA}$

spectrum is not unlike that found in glass work [21].

To monitor the ratio of the integrated fluorescence intensities we designated the band intensity (i.e., that part of the spectrum below the peaks) as I_B , which are the activator sites and the remaining portion as I_{NB} , NB denotes nonband, which are the sensitizer sites. Figure 10 shows the time evolution of the ratio of the integrated intensities, I_B/I_{NB} . Table III lists the data plotted in Figure 10.

The simple discrete site model used here is again an interacting three level system but this time we assume negligible or no back transfer [21]. Figure 11 depicts this situation. This model is generalized for three sites denoted as site 1, site 2, and site 3. Since we choose to use this model for $\text{La}_{.5}\text{Pr}_{.5}\text{P}_5\text{O}_{14}$ at 50K and $\text{PrP}_5\text{O}_{14}$ at 12K and the identification of the appropriate site with a given energy peak will be made at a later time. The rate equations of the populations for the three sites are

$$dn_1/dt = W_1 - \beta_1 n_1 - \omega_{12} n_1 \quad (14a)$$

$$dn_2/dt = W_2 - \beta_2 n_2 + \omega_{12} n_1 - \omega_{23} n_2 \quad (14b)$$

$$dn_3/dt = W_3 - \beta_3 n_3 + \omega_{23} n_2 \quad (14c)$$

Assuming the transfer rate is time independent (not a necessary condition) and using the method of Laplace transforms, the ratio of intensities for this situation is

$$\frac{I_2}{I_3} = \frac{\frac{\beta_2^r}{\beta_3^r} \{A \exp[-(\beta_2 + \omega_{23})t] - B \exp[-(\beta_1 + \omega_{12})t]\}}{C \exp(-\beta_3 t) + D \exp[-(\beta_2 + \omega_{23})t] + E \exp[-(\beta_1 + \omega_{12})t]} \quad (15)$$

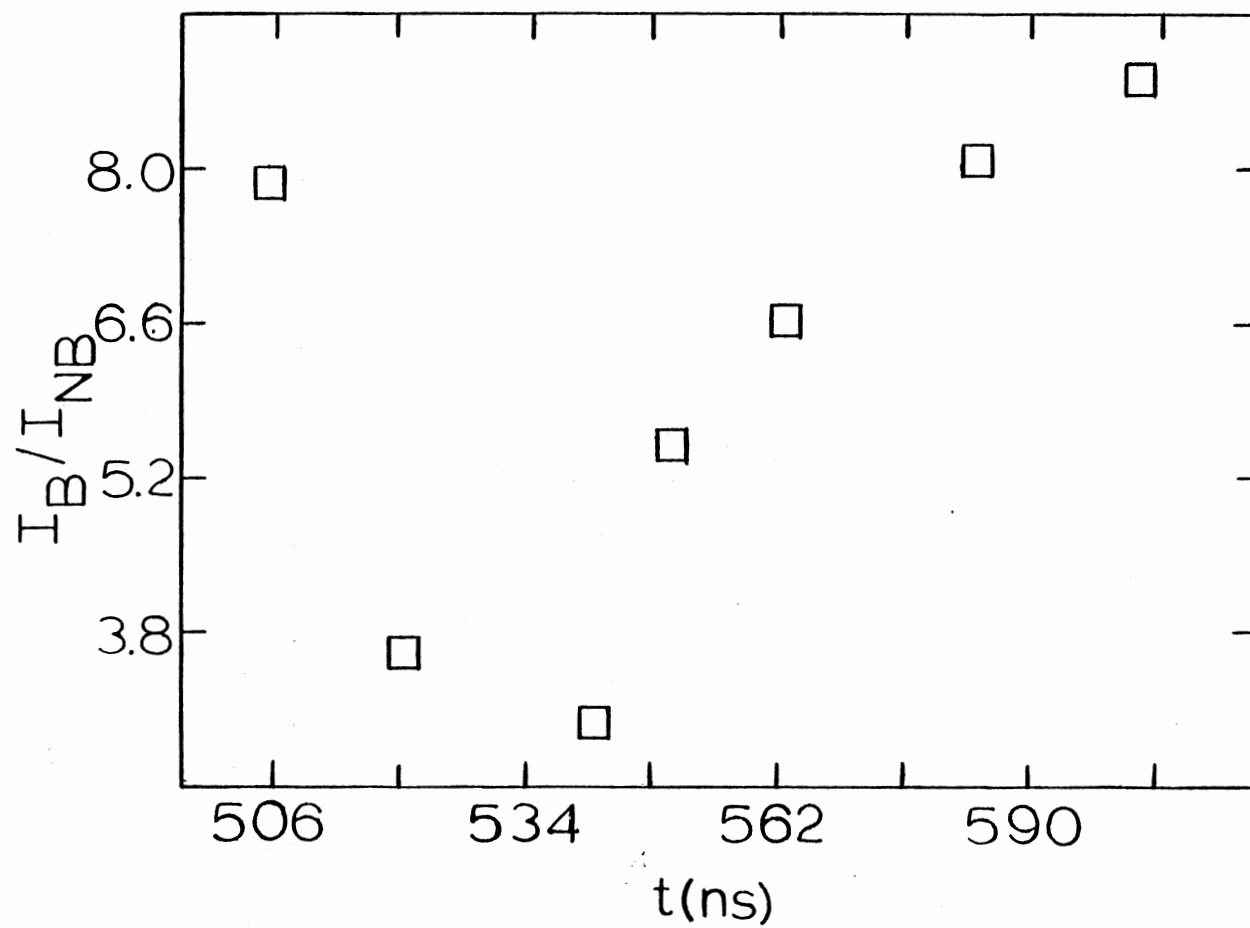


Figure 10. Time Evolution of the Ratio of the Intensities for $\text{La}_{0.5}\text{Pr}_{0.5}\text{P}_5\text{O}_{14}$ at 50K

TABLE III

RATIO OF INTENSITIES AND TIME AFTER
PULSE FOR $\text{La}_{.5}\text{Pr}_{.5}\text{P}_5\text{O}_{14}$ AT 50K

T_{ap} (ns)	$I_{\text{B}}/I_{\text{NB}}$
506.0	7.90
520.0	3.60
540.0	2.97
548.0	5.50
560.0	6.65
580.0	8.10
600.0	8.84

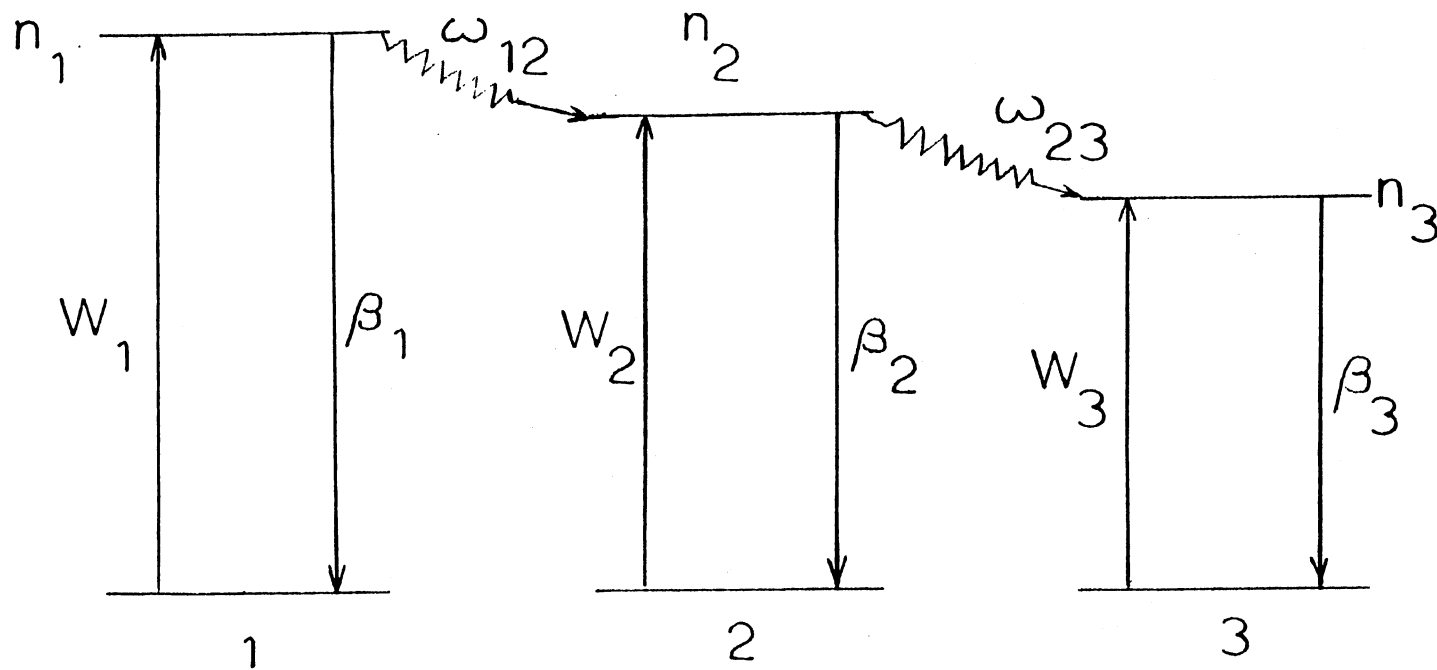


Figure 11. Proposed Energy Transfer Model for $\text{La}_{.5}\text{Pr}_{.5}\text{P}_5\text{O}_{14}$ at 50K and $\text{PrP}_5\text{O}_{14}$ at 12K

where

$$A = n_2(0) + \omega_{12}n_1(0)/(\beta_1 - \beta_2 + \omega_{12} - \omega_{23})$$

$$B = \omega_{12}n_1(0)/(\beta_1 - \beta_2 + \omega_{12} - \omega_{23})$$

$$C = n_3(0) + \left[\frac{\omega_{23}\omega_{12}n_1(0)}{(\beta_1 - \beta_3 + \omega_{12})(\beta_1 - \beta_2 + \omega_{12} - \omega_{23})} \right] \\ - \left[\frac{\omega_{23}n_2(0) + \omega_{23}\omega_{12}n_1(0)/(\beta_1 - \beta_2 + \omega_{12} - \omega_{23})}{(\beta_2 - \beta_3 + \omega_{23})} \right]$$

$$D = \left[\frac{\omega_{23}n_2(0) + \omega_{23}\omega_{12}n_1(0)/(\beta_1 - \beta_3 + \omega_{12} - \omega_{23})}{(\beta_2 - \beta_3 + \omega_{23})} \right]$$

$$E = \omega_{23}\omega_{12}n_1(0)/(\beta_1 - \beta_3 + \omega_{12})(\beta_1 - \beta_2 + \omega_{12} - \omega_{23})$$

Here we make the identification $I_2/I_3 = I_B/I_{NB}$, i.e., site 2 represents the continuum of sites in the band (activators) and site 3 represents the nonband or peaks (sensitizers). The reason sites 2 and 3 were chosen for this representation was based upon the use of this model for the PrP_{514} at 12K whose data had a similar time evolution of the intensity ratio, that is to say, we initially chose this model for PrP_{514} at 12K but it also may apply here. The data listed in Table III has yet to be fitted to Eq. (15).

PrP_{514} Analysis

This stoichiometric sample at 12K exhibits a spectrum with two peaks, high energy at 6072.3\AA , low energy at 6075.2\AA and a shoulder (small peak) in the low energy wing on the low energy side. The lifetime of the high energy peak is 311 ns and that of the low energy peak is 350 ns. It is assumed that the lifetime of the shoulder is approximately that of the low energy peak. This excitation wavelength

(approximately $4812\overset{\circ}{\text{A}}$) excites the three sites and as time evolves the spectral intensities shift among the peaks and wings. Figure 12 shows the spectral dependence on the time after pulse for $\text{PrP}_{514}^{\text{O}}$ at 12K. The fluorescence spectra at two different excitation wavelengths is shown in Figure 13. This shows we can selectively excite Pr^{3+} ions in nonequivalent crystal sites.

The time evolution of the integrated intensities involves two graphs: i) $I_{\text{H}}/I_{\text{L}}$ vs time and ii) $I_{\text{L}}/I_{\text{S}}$ vs time. This data is presented in Table IV and the graphs are shown in Figures 14 and 15. In comparing Figures 14 and 15 we see at short times after pulse $I_{\text{H}}/I_{\text{L}}$ is increasing while $I_{\text{L}}/I_{\text{S}}$ is decreasing indicating that energy is being transferred from the high energy peak to the low energy. At approximately 227 ns, the reverse is initiated and $I_{\text{H}}/I_{\text{L}}$ decreases while $I_{\text{L}}/I_{\text{S}}$ increases indicating transfer from the low energy site to the shoulder. Finally at long times after pulse the energy transfer reaches equilibrium.

The interacting three level system presented in the last section is ideal in modeling this system. From the rate equations, Eqs. (14), the ratio of the intensities $I_{\text{H}}/I_{\text{L}}$ is given by

$$\frac{I_1}{I_2} = \frac{(\beta_1^r/\beta_2^r)n_1(0)\exp[-(\beta_1 + \omega_{12})t]}{A\exp[-(\beta_2 + \omega_{23})t] - B\exp[-(\beta_1 + \omega_{12})t]} \quad (16)$$

where

$$A = n_2(0) + \omega_{12}n_1(0)/(\beta_1 - \beta_2 + \omega_{12} - \omega_{23})$$

$$B = \omega_{12}n_1(0)/(\beta_1 - \beta_2 + \omega_{12} - \omega_{23})$$

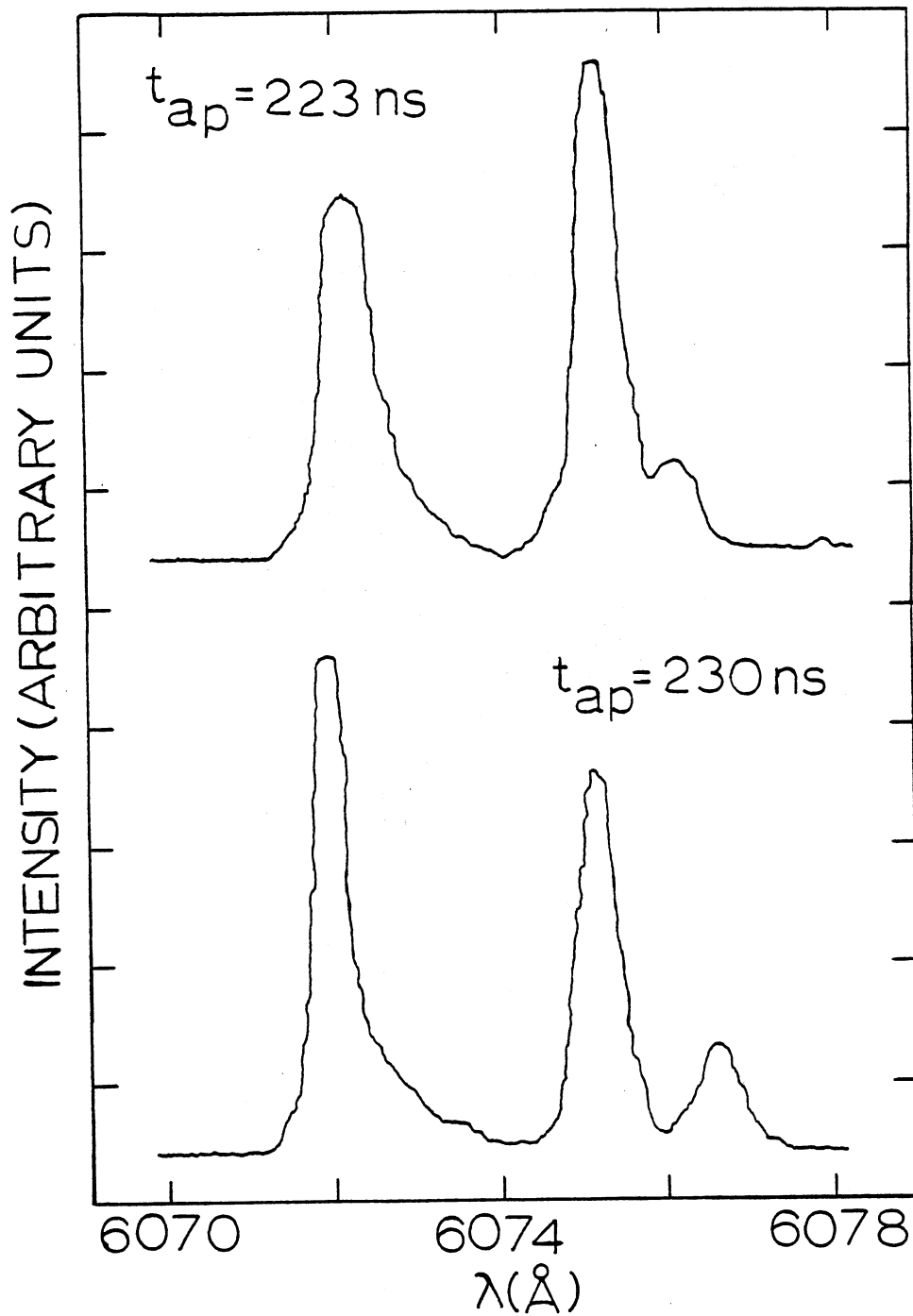


Figure 12. Spectral Dependence on Time After Pulse for $\text{PrP}_{514}\text{O}_{14}$ at 12K and $\lambda_x = 4812 \text{\AA}$

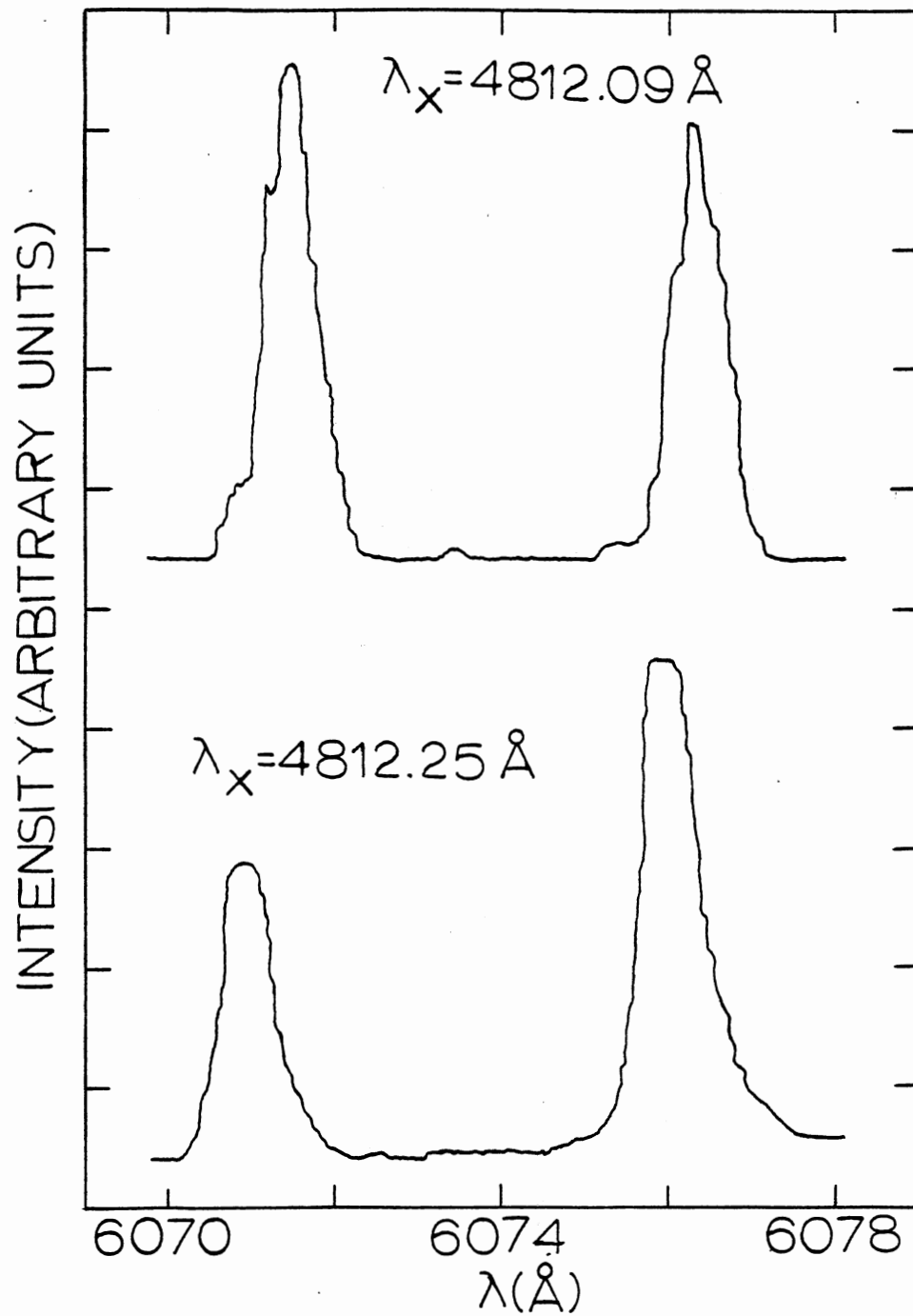


Figure 13. Fluorescence Spectra of PrP5O₁₄ at Two Different Excitation Wavelengths and $t_{ap} = 214 \text{ ns}$

TABLE IV

RATIO OF INTENSITIES AND TIME AFTER PULSE FOR $\text{PrP}_{514}^{\text{O}}$ AT 12K

t_{ap} (ns)	$I_{\text{H}}/I_{\text{L}}$	$I_{\text{L}}/I_{\text{S}}$
223.0	1.04	13.7
224.0	1.12	7.71
225.0	1.42	6.98
226.0	1.43	6.98
227.0	1.49	5.99
228.0	1.61	4.93
229.0	1.49	4.98
230.0	1.43	3.50
231.0	1.07	4.24
232.0	1.41	4.00
234.0	1.13	8.54
236.0	1.12	12.6
240.0	1.10	13.7
260.0	.985	13.6
280.0	.864	14.0
340.0	.945	13.6
400.0	1.12	14.0

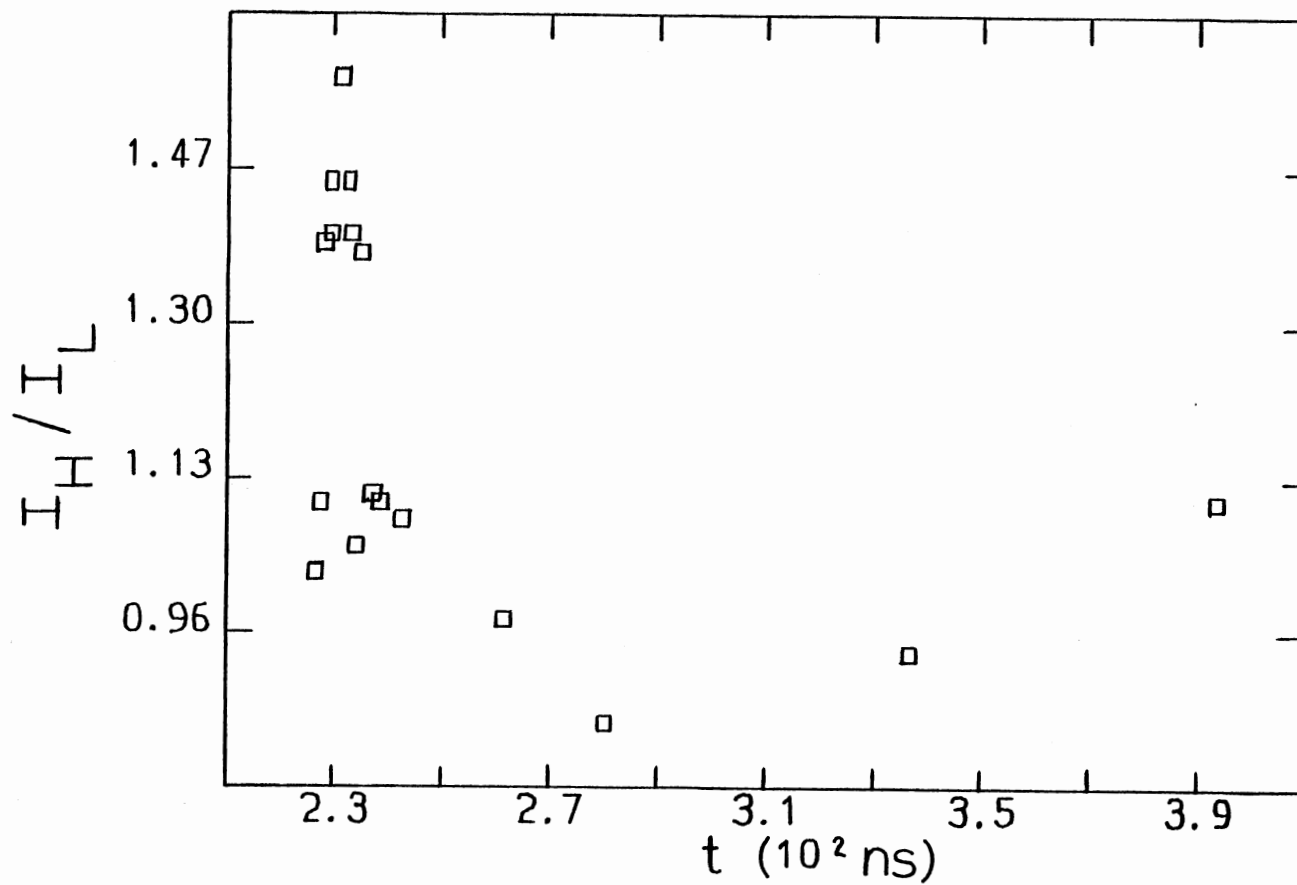


Figure 14. Time Evolution of the Ratio I_H/I_L for PrP_{514} at 12K

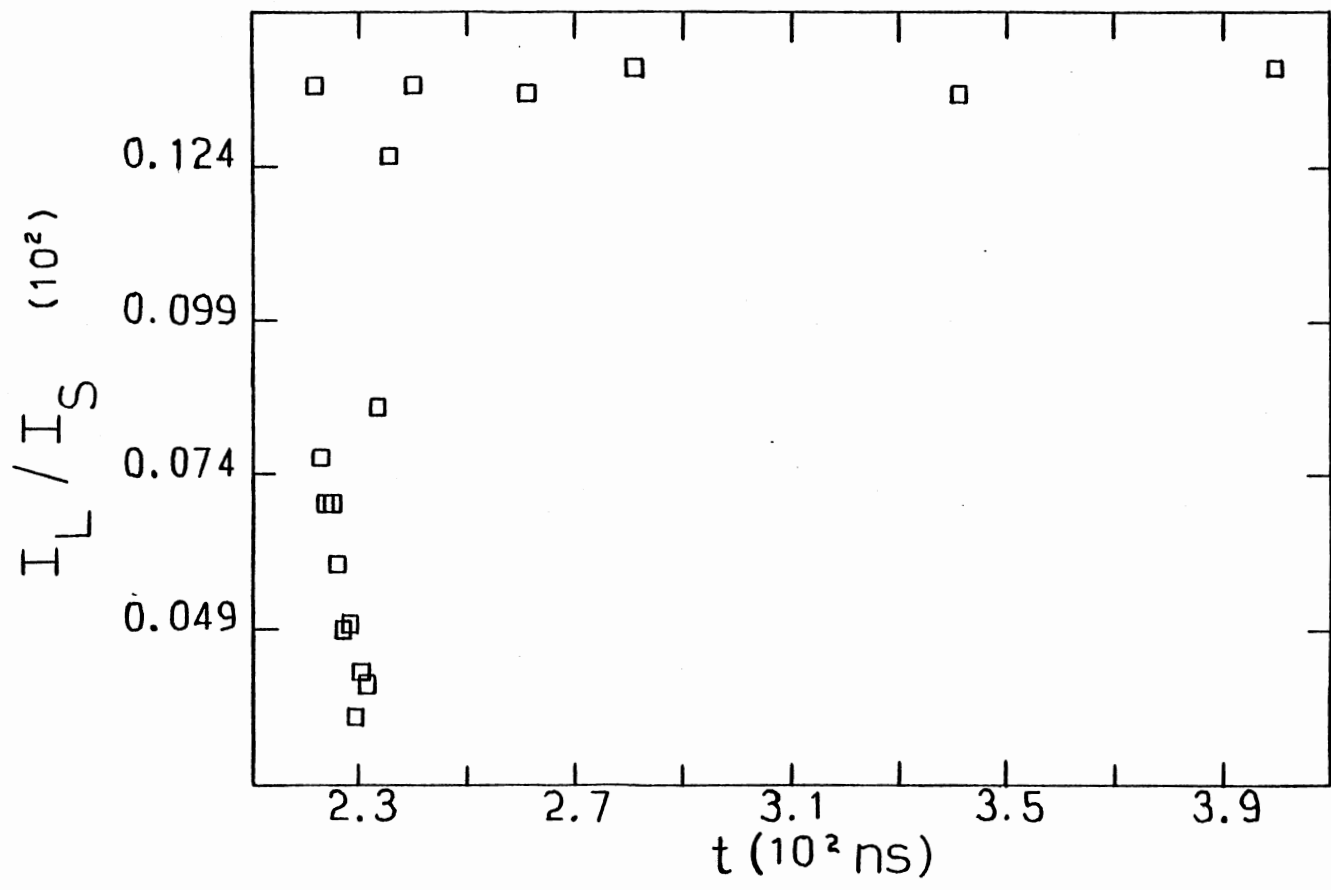


Figure 15. Time Evolution of the Ratio I_L / I_S for $\text{PrP}_{514}\text{O}_{14}$ at 12K

and Eq. (15) would represent the ratio I_L/I_S . Thus, we have assigned the high energy peak to site 1, the low energy peak to site 2, and the shoulder to site 3. As mentioned earlier the similarity of Figures 10 and 15 in part determined the use of this model for $\text{La}_{.5}\text{Pr}_{.5}\text{P}_5\text{O}_{14}$ at 50K. The data in Table IV has yet to be fitted to Eqs. (15) and (16).

At 48K the spectra of $\text{PrP}_5\text{O}_{14}$ exhibits two peaks; an example of the spectrum at short and long times after pulse is illustrated in Figure 16. The laser pumps these two sites, as time increases the energy migrates from the low energy peak (sensitizer) to the high energy peak (activator). The lifetime of the high energy peak is 312 ns and that of the low energy peak is 316 ns. The time evolution of the ratio of the integrated intensities I_L/I_H is shown in Figure 17. This data is listed in Table V.

To model this behavior we return to the interacting two-level system with time independent transfer rates with back transfer and equal lifetimes. This is depicted in Figure 7. The solution of the rate equations, Eqs. (9), gives us Eq. (10) for the ratio of the intensities. The data in Table V has yet to be fitted to Eq. (10).

$\text{La}_{.9}\text{Pr}_{.1}\text{P}_5\text{O}_{14}$ Analysis

This mixed crystal was investigated only at 12K. This spectrum exhibits two peaks. The lifetime of the high energy peak is 282 ns and that of the low energy peak is 270 ns. Figure 18 depicts the fluorescence spectra at two different excitation wavelengths indicating that Pr^{3+} ions are situated in nonequivalent crystallographic sites. Figure 19 shows the spectral dependence on time after pulse. The ratio of the integrated intensities I_H/I_L versus time after pulse is illustrated in

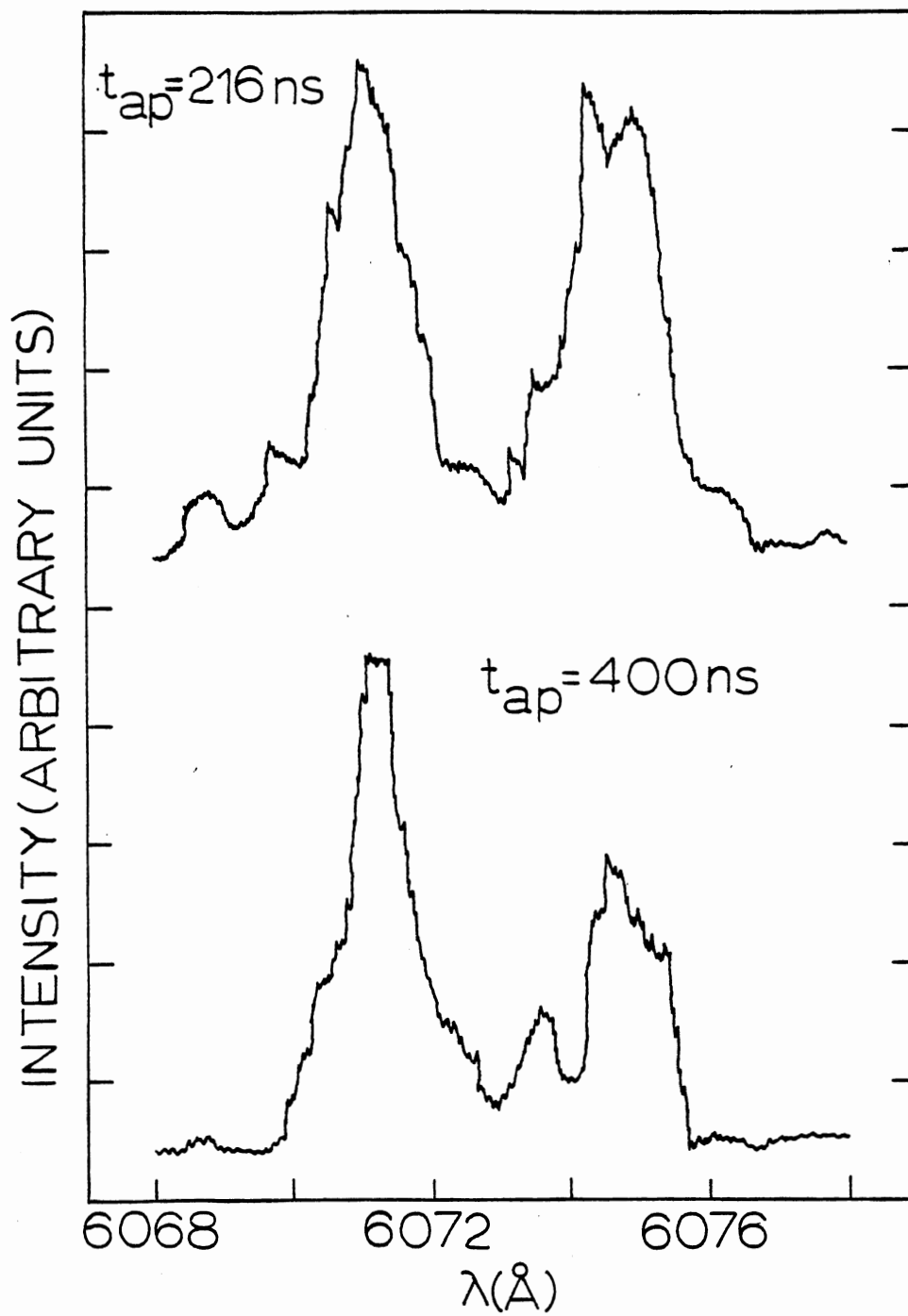


Figure 16. Spectral Dependence on Time After Pulse for $\text{PrP}_{514}\text{O}_{14}$ at 48K and $\lambda_x = 4812\text{\AA}$

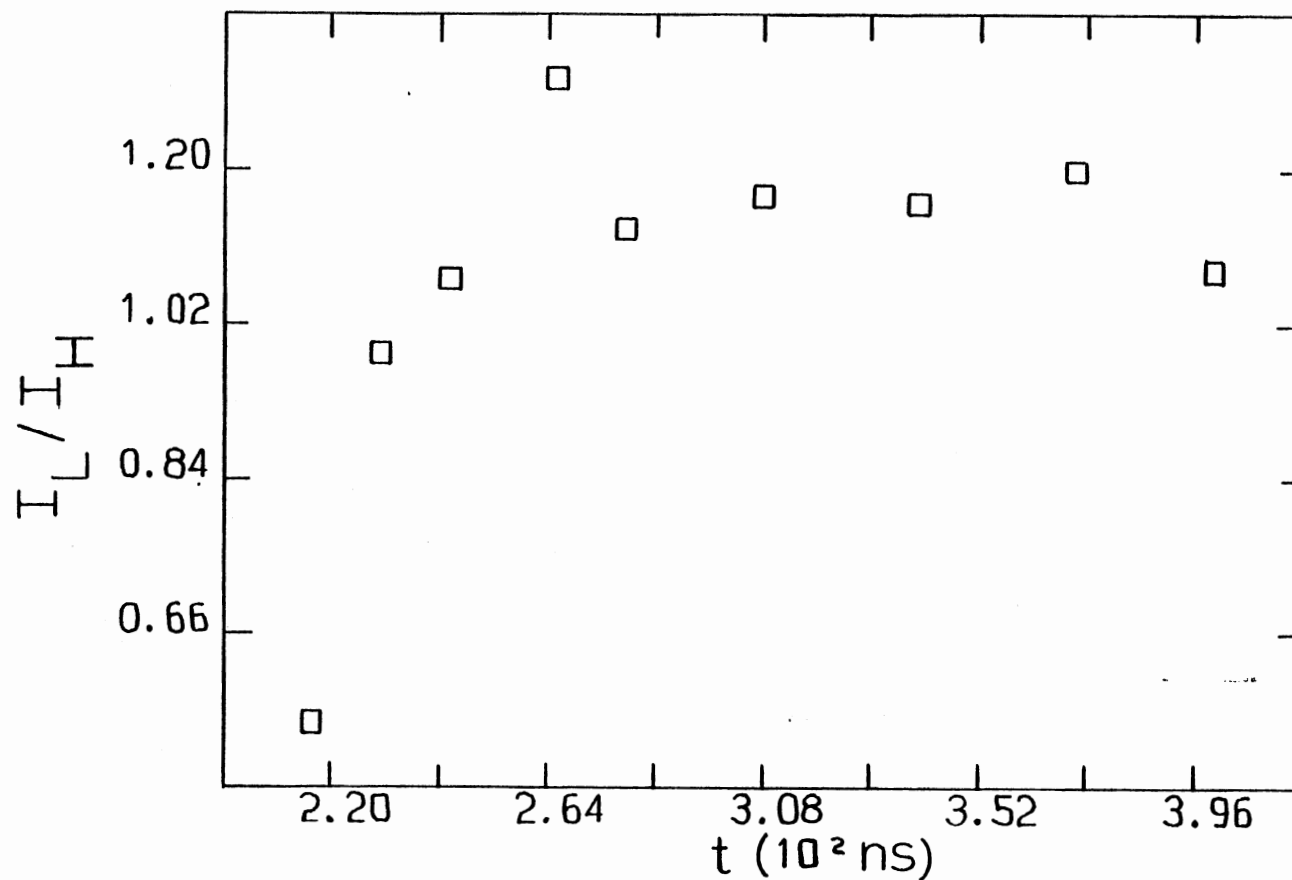


Figure 17. Time Evolution of the Ratio I_L/I_H for PrP_{514}O at 48K

TABLE V
RATIO OF INTENSITIES AND TIME AFTER PULSE
FOR PrP_{514}O AT 48K

t_{ap} (ns)	$I_{\text{L}}/I_{\text{H}}$
216.0	0.555
230.0	1.00
244.0	1.09
266.0	1.33
280.0	1.15
308.0	1.19
340.0	1.18
372.0	1.22
400.0	1.10

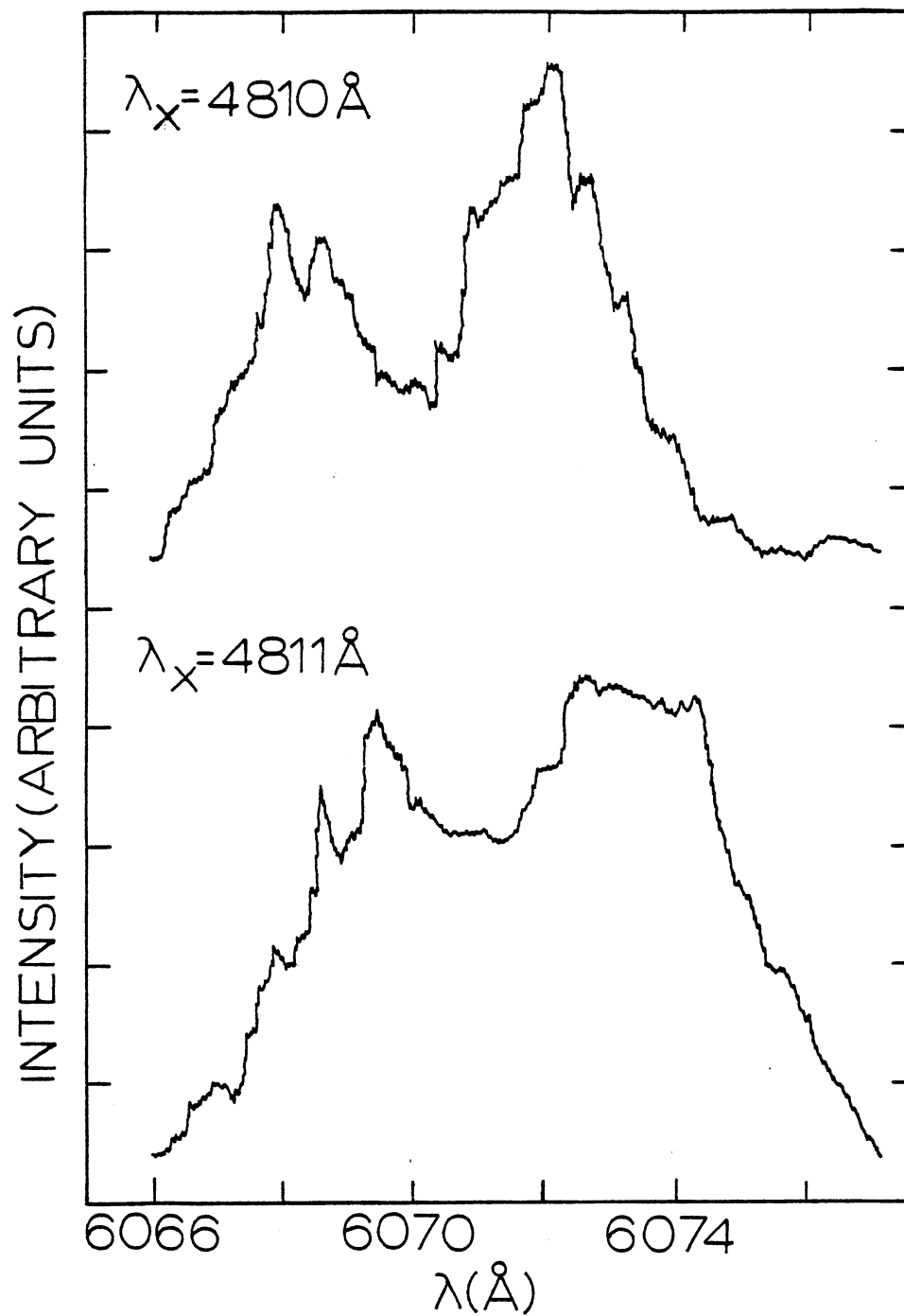


Figure 18. Fluorescence Spectra of $\text{La}_{0.9}\text{Pr}_{0.1}\text{P}_5\text{O}_{14}$ at Two Different Excitation Wavelengths at $t_{\text{ap}} = 278\text{ns}$

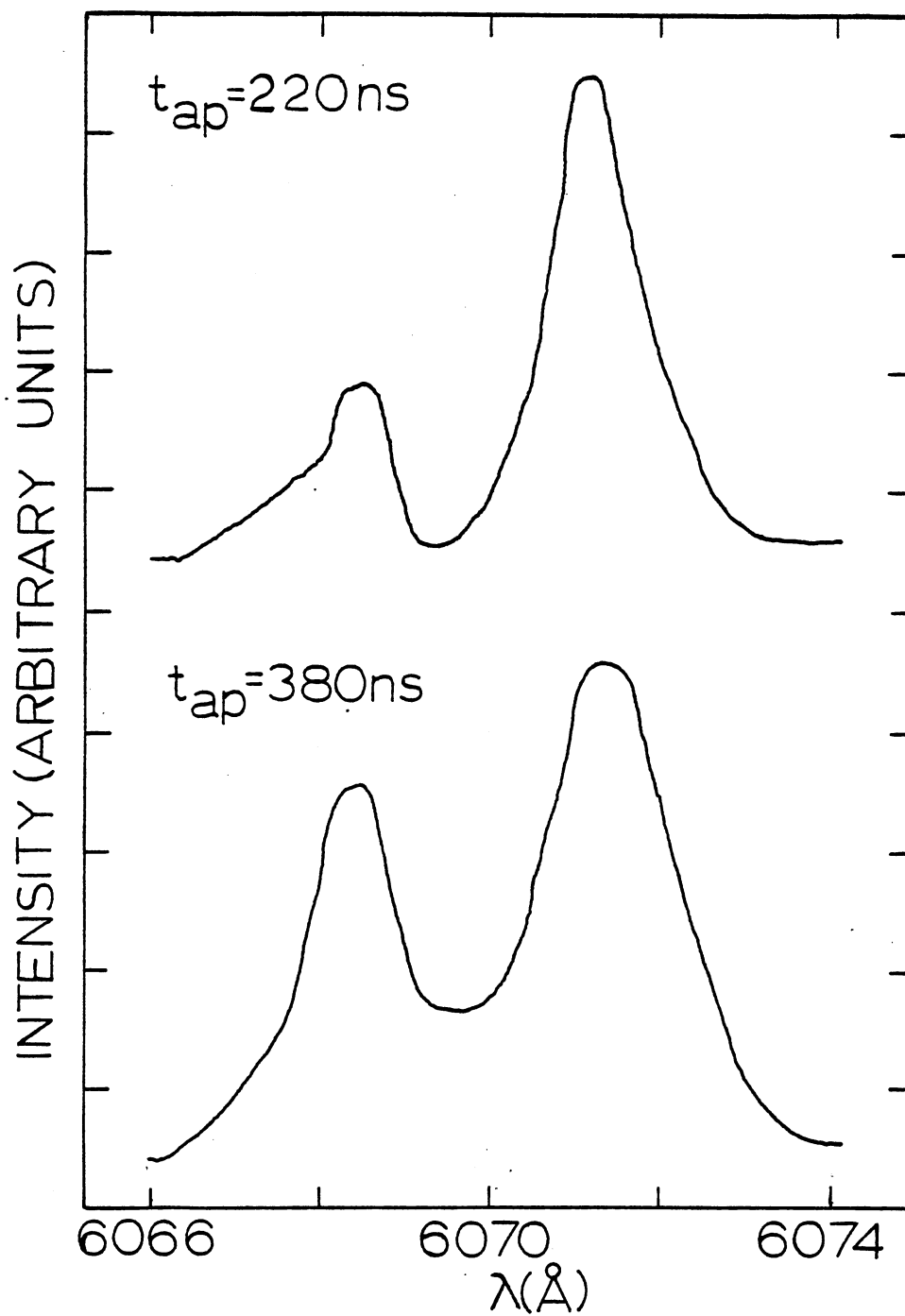


Figure 19. Spectral Dependence on Time After Pulse for $\text{La}_{0.9}\text{Pr}_{0.1}\text{P}_5\text{O}_{14}$ at 12K and $\lambda_x = 4806\text{\AA}$

Figure 20 and the data is listed in Table VI. We see that Figure 20 looks similar to that of Figure 14. The tendency here is to use the interacting three-level model previously introduced, but the structure of the spectra indicate that this model may be inappropriate. We have yet to determine a model for this sample [21].

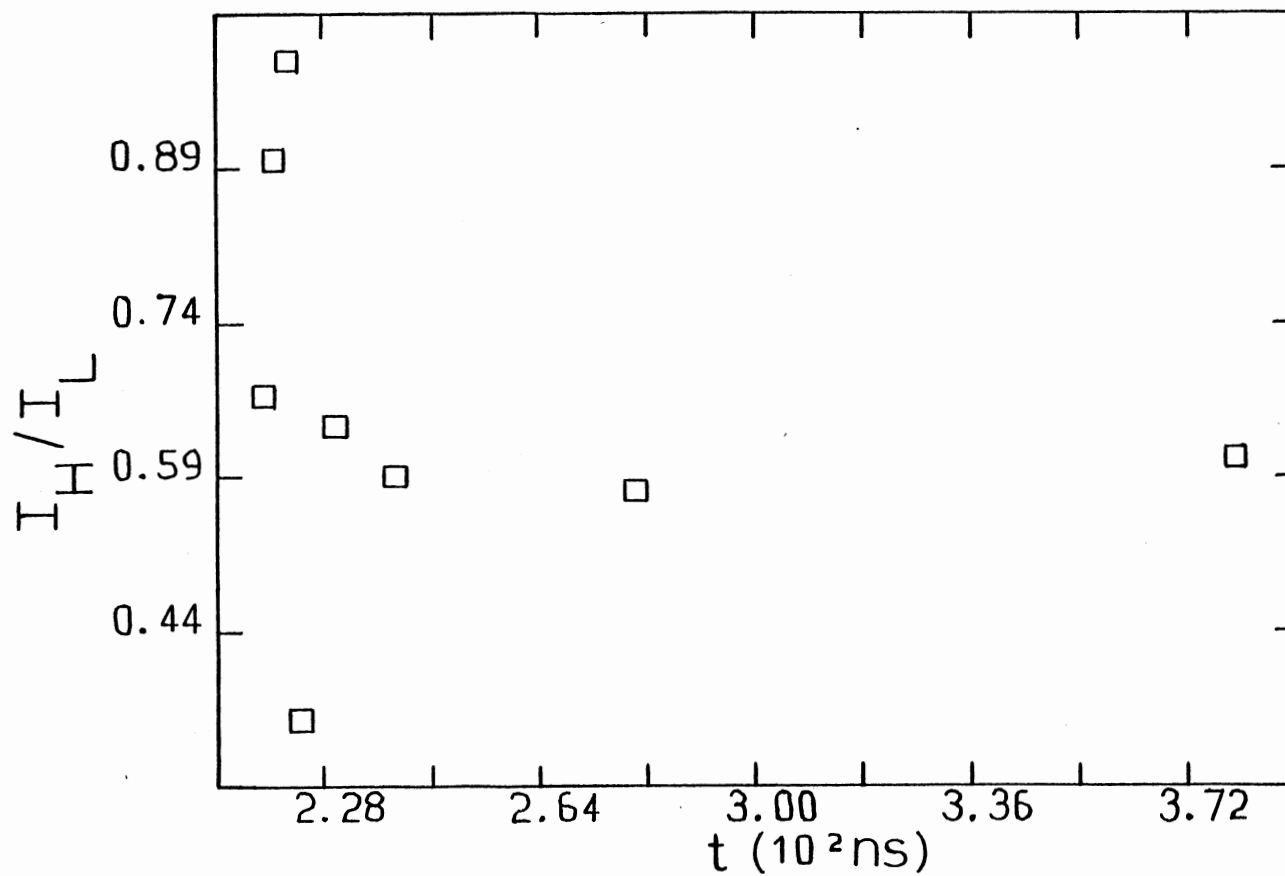


Figure 20. Time Evolution of the Ratio I_H/I_L for $\text{La}_{0.9}\text{Pr}_{0.1}\text{P}_5\text{O}_{14}$ at 12K

TABLE VI
RATIO OF INTENSITIES AND TIME AFTER PULSE
FOR $\text{La}_{.9}\text{Pr}_{.1}\text{P}_5\text{O}_{14}$

t_{ap} (ns)	$I_{\text{H}}/I_{\text{L}}$
218.0	.669
330.0	.898
222.0	.994
224.0	.352
230.0	.640
240.0	.590
280.0	.575
380.0	.608

CHAPTER V

SUMMARY AND CONCLUSIONS

The mixed crystals of $\text{La}_{1-x}\text{Pr}_x\text{P}_5\text{O}_{14}$ ($x = 0.5$ and $x = 0.1$) and the stoichiometric sample $\text{PrP}_5\text{O}_{14}$ were investigated using the techniques of optical excitation and emission at 12K, and site selection spectroscopy at 12K and approximately 50K. The site selection spectroscopy showed that in each sample the spectrum was dependent upon laser excitation wavelength, indicating that the Pr^{3+} ions were in nonequivalent crystallographic sites. The time evolution of the spectra indicate that energy transfer is taking place. Unsuccessful attempts were made at fitting the data to two previously existing models for $\text{La}_{.5}\text{Pr}_{.5}\text{P}_5\text{O}_{14}$ at 12K. Other energy transfer models for $\text{La}_{.5}\text{Pr}_{.5}\text{P}_5\text{O}_{14}$ and $\text{PrP}_5\text{O}_{14}$ have been proposed. A model for the $\text{La}_{.9}\text{Pr}_{.1}\text{P}_5\text{O}_{14}$ is under debate.

According to Dornauf and Heber [6], in strongly doped crystals with $x \geq 0.3$ only fluorescence from the $^3\text{P}_0$ term is detectable, whereas in highly dilute crystals almost the whole fluorescence starts from the $^1\text{D}_2$ level. The data reported here essentially agrees with Dornauf and Heber's work but it should be noted that no $^1\text{D}_2$ transitions were detected in general and specifically not in the $x = 0.1$ sample. Since a $^1\text{D}_2$ level is a metastable state it has a long lifetime (minimum of 5 microseconds [6]) and ushc a long lifetime has not been seen in these samples.

For $^3\text{P}_0$ fluorescence lifetime measurements, there is a great

discrepancy between this work and that of Dornauf and Heber. They report 124 ± 6 ns lifetimes for all samples ($0.001 \leq x \leq 1$) at 4.2K; and at 77K, the dilute samples, up to $x = 0.15$, are approximately 139 ns and for $x \geq 0.15$ are 124 ns. The only thing we agree on is that the lifetimes are purely exponential.

Dornauf and Heber [6] found that the frequently employed Inokuti-Hirayama continuum approximation fails when analyzing the time-resolved fluorescence of the 1D_2 level. Only if the particular structure of the pentaphosphates is taken into account is it then possible to determine the dipole-quadrupole character of the ion-ion interaction. They show because of the lack of spectral diffusion and the good fit of the time-resolved fluorescence to a direct energy transfer model without energy migration, that there is no resonant diffusion of excitation energy in $\text{La}_{1-x}\text{Pr}_x\text{P}_5\text{O}_{14}$.

This seems consistent with the discrete site, single step models we have proposed. The energy transfer interaction should be a multipole-multipole interaction as opposed to an exchange interaction because of the crystal structure [22]; no Pr^{3+} ions are linked by oxygen ions. This is also confirmed by Dornauf and Heber [6].

Discussions with Boulon [23] have suggested that the activity in the wings of the spectra are satellite lines due to pairs of neighboring Pr^{3+} ions coupled by dipolar or quadrupole interactions [24].

Future work should consist of fitting the data to the proposed models, finding a model for the $\text{La}_{.9}\text{Pr}_{.1}\text{P}_5\text{O}_{14}$ sample, and the determination of the energy parameters along with the determination of the temperature dependence on the lifetimes and energy transfer. Additional work could include up conversion.

REFERENCES

1. Lawson, Christopher M. Studies of Spectral and Spatial Energy Transfer in Solids. Ph.D. Thesis, Oklahoma State University, 1981.
2. Merkle, Larry D. Energy Transfer in Europium Doped Potassium Chloride. M.S. Thesis, Oklahoma State University, 1976.
3. Yariv, A. Quantum Electronics, 2nd Ed., Wiley, New York, 1975.
4. Weber, M. J. Rare Earth Lasers, In: Gschneider and Eyring, Ed., Handbook on the Physics and Chemistry of Rare Earths, North-Holland Pub. Co., Amsterdam, 1979.
5. Dornauf, H. and J. Heber. J. of Luminescence 20, 271 (1979).
6. Dornauf, H. and J. Heber. J. of Luminescence 22, 1 (1980).
7. Powell, R. C. and G. Blasse. Structure and Bonding 42, 43 (1980).
8. Förster, T. Ann. Phys. 2, 55 (1948); Z. Naturforsch 49, 321 (1949).
9. Dexter, D. L. J. Chem. Phys. 21, 836 (1953).
10. Inokuti, M., F. Hirayama. J. Chem. Phys. 43, 1978 (1965).
11. Holstein, T., S. K. Lyo and R. Orback. In: Laser Spectroscopy of Solids (Eds. W. M. Yen, P. M. Selzer) Springer-Verlag, New York, 1981, page 39.
12. Miyakawa, T., D. L. Dexter. Phys. Rev. B1, 2961 (1970).
13. Soos, Z. G., R. C. Powell. Phys. Rev. B6, 4035 (1972).
14. Chow, H. C., R. C. Powell. Phys. Rev. B21, 3785 (1980).
15. Yokota, M., O. Tanimoto. J. Phys. Soc. Japan 22, 779 (1967).
16. Burshstein, A. I. Sov. Phys. JETP 35, 882 (1972).
17. Lawson, Christopher M., Edwin E. Freed, Richard C. Powell. J. Chem. Phys. 76(8), 15 (1982).
18. Merkle, Larry D. and R. C. Powell. Phys. Rev. B 20, 75 (1979).

19. Smith, W. Bryan and R. C. Powell. J. Chem. 76(2), 15 (1979).
20. Tyminski, Jacek K., Christopher M. Lawson and Richard C. Powell.
To be published in Journal of Chemical Physics.
21. Powell, Richard C. Private Communication.
22. Bagieu-Beucher, M. Duc Tranqui. Bull. Soc. Fr. Mineral. Cristallogr. 93, 505 (1970).
23. Boulon, George. Private Communication.
24. Vial, J. C., R. Buisson, F. Madeore and M. Poirier. Le Journal De Physique 40, 913 (1979).

VITA

Robert Bruce Ruokolainen
Candidate for the Degree of
Master of Science

Thesis: THE STUDY OF SPECTRAL ENERGY TRANSFER IN $\text{La}_{1-x}\text{Pr}_x\text{P}_5\text{O}_{14}$

Major Field: Physics

Biographical:

Personal Data: Born in Highland Park, Michigan, March 31, 1952, the son of Mr. Richard B. Ruokolainen and Mrs. Allene M. Ruokolainen.

Education: Graduated from Franklin High School, Livonia, Michigan, in June 1970; received Bachelor of Science degree from Eastern Michigan University in December, 1974; graduated with a Master of Science degree from Eastern Michigan University in June, 1980; completed requirements for the Master of Science degree from Oklahoma State University, December, 1982.

Professional Experience: Electronics Laboratory Assistant, Department of Physics, Eastern Michigan University, 1976; physics tutor, Department of Physics, Eastern Michigan University, 1976-1977; graduate teaching assistant, Department of Physics, Eastern Michigan, 1977-1980; graduate teaching assistant, Department of Physics, Oklahoma State University, 1980-1981; research assistant, Department of Physics, Oklahoma State University, 1981-1982.